Tunable Microchips for Imaging Protein Structures Formed in Breast Cancer Cells

Nicholas Andrew Alden

Thesis submitted to the faculty of the Virginia Polytechnic Institute and State University in partial fulfillment of the requirements for the degree of

Master of Science
In
Mechanical Engineering

Deborah F. Kelly. Chair
Amrinder S. Nain
Bahareh Bekham

2/20/2018
Blacksburg, Virginia

Keywords: Cryo-Electron Microscopy, BRCA1, p53, Silicon Nitride Microchips

Tunable Microchips for Imaging Protein Structures Formed in Breast Cancer Cells

Nicholas Alden

ABSTRACT

The breast cancer susceptibility protein, BRCA1, is a tumor suppressor that helps maintain genomic integrity. Changes in BRCA1 that effect DNA repair processes can fuel cancer induction. The Kelly lab, at the Virginia Tech Carilion Research Institute, has recently developed a new methodology that employs silicon nitride (SiN) microchips to isolate BRCA1 assemblies from the nuclear material of breast cancer cells. These microchips are coated with adaptor proteins that include antibodies against target proteins of interest. The adaptor proteins are added in sequential steps to the coated microchips, followed by an aliquot of sample containing the protein of interest, such as BRCA1. The Kelly lab, partnered with Protochips Inc., developed these devices as a robust, tunable platform to monitor molecular processes, and refer to them as "Cryo-SiN" in cryo-Electron Microscopy (EM) imaging. We are currently using Cryo-SiN to recruit BRCA1 protein assemblies to the microchip surface under mild conditions, while simultaneously preparing them for cryogenic preservation and EM imaging. This strategy presents a viable alternative to antibody affinity columns that require stringent elution steps to obtain protein complexes from the column. Another advantage of the microchip strategy is that it requires only a 30-minute nuclear extraction, a 60-minute enrichment procedure, and a 5-minute microchip capture step – a total of 95 minutes from initially lysing the cells to plunge-freezing the EM specimens. Therefore, these novel approaches represent a major departure from classical separation procedures that often require days to complete, during which time active protein assemblies can readily dissociate or become inactive. Overall, our use of BRCA1-specific microchips may reveal changes in the BRCA1 architecture during various stages of cancer progression – a major gap in knowledge that persists in cancer research.

Tunable Microchips for Imaging Protein Structures Formed in Breast Cancer Cells

Nicholas Alden

GENERAL AUDIENCE ABSTRACT

Modern advances in the imaging technology used for cryogenic electron microscopy (cryo-EM) have offered researchers an extraordinary view into the world of biology at the nanoscale. Supplemental to these technical innovations is the development of tunable substrates based on functional new materials that revolutionize the sequestering of biological components from human cells, such as protein complexes formed in breast cancer cells. New developments of novel viewing substrates, given traditional electron microscopy viewing grids have remained unchanged for decades, is the logical next step into the future of enhanced cryo-EM imaging. Tunable microchip substrates, made using recently enhanced micro-engineering techniques, are currently under development for use in cryo-EM imaging. In this work I have examined these microchip substrates for their capacity to streamline the isolation of biomolecules such as the protein most prominently cited in breast cancer, known as the breast cancer susceptibility protein (BRCA1). Utilizing these novel microchip substrates in the Kelly Lab, I have collected and analyzed data containing BRCA1 proteins, formed in human breast cancer cells, toward the development of 3-dimensional protein structures that allow us to peer into the structure-function relationships of these proteins. New and exciting Cryo-EM data, collected using these newly developed microchips, has the potential to reveal obscure disease mechanisms being propagated at the molecular level in modern clinical practice, such as breast cancer.

ACKNOWLEDGMENTS:

This research is supported by development funds from Virginia Tech, the Commonwealth Health Research Board (2080914), the Concern Foundation (303872), and NIH/NCI (R01CA193578) to D.F.K.

TABLE OF CONTENTS

LIST OF FIGURES

LIST OF TABLES

INTRODUCTION:

The Kelly lab, at the Virginia Tech Carilion Research Institute (VTCRI), studies the structure/function relationship of breast cancer susceptibility protein (BRCA1) complexes, which are highly implicated in the development of breast and ovarian cancer. Single particle Electron Microscopy (EM), specifically cryogenic EM (cryo-EM), allows the Kelly lab to look at these BRCA1 complexes at resolutions on the order of approximately 10 to 15 angstroms (Å) to provide further insight into the 3-Dimensional (3D) structure of biomolecules and proteins.

BRCA1 is a gene that encodes a protein of 1863 amino acids. It has two highly conserved motifs being the N-terminal RING domain and the tandem C-terminal BRCT domains. It has been established that the RING domain convenes the E3 ubiquitin ligase activity through encoding a folded protein framework, and that the BRCT domain is responsible for binding the phosphorylated protein substrates predominantly involved in DNA damage repair.

In the nucleus, BRCA1 collaborates with its binding partner BRCA1-associated RING domain protein 1 (BARD1). BARD1 encodes a protein of 777 amino acids that also contains an N-terminal RING domain and a C-terminal BRCT domain. These two (RING and BRCT) domains have been determined via NMR spectroscopy and X-Ray crystallography methods to reveal part of BRCA1's three dimensional architectures, yet the full-length structure of BRCA1 has remained largely unknown until recently. Within the cell nucleus, the BRCA1-BARD1 heterodimer works to repair DNA lesions through interactions with other known repair proteins. Mutations inherited in the BRCA1 gene often leads to operative insufficiencies. When experiencing excessive oxidative stress, cells undersupplied with functional BRCA1 will begin to accrue biochemical affronts known to trigger the induction of cancer.

The Kelly lab, through cryo-EM techniques accompanied by the use of statistical classification and averaging routines, developed the first full-length structure of BRCA1 proteins and complexes formed in human breast cancer cells. These full length BRCA1 complexes exhibited a C-shaped, clamp-like motif with the RING domain at one end, tandem BRCT domains at the other end, and a flexible core region bridging the two. At the molecular level, it remains inadequately understood how stress inducing scenarios or environmental changes affect BRCA1 and its ability to adapt and maintain DNA damage repair events. Remaining issues are, how is the structure-function relationship of BRCA1 affected by mutations, and will it be possible to repair BRCA1 assemblies that are affected by such mutations? Further, can mutated BRCA1's natural function be restored?

Combining structural biology and biochemical tools has allowed for us to begin confronting these questions. The use of single particle EM permits us to investigate structural variances between BRCA1-BARD1 originated from different human breast cancer cell lines. BRCA1-BARD1 assemblies formed in both mutated and wild type cell lines produced highly similar 3D structures. Differences between the structures reside in the degron region proximal to the N-terminal RING domain. This region is dubbed a modification "hot spot" by Dr. Kelly and members of her lab. Using biochemical tools, ubiquitin moieties in this modification "hot spot" region were removed and mutated BRCA1's structure was restored to normal. My contribution to the next phase of work examines BRCA1 assemblies isolated on tunable microchips.

The specific cell line used in the studies outlined in this document, known as MDA-MB-361 (ATCC), have been shown to exhibit differences in the C-terminal BRCT domain through negative stain techniques. Negatively stained samples produced 3D structures with a significantly enlarged BRCT domain, believed to be the presence of a partner binding protein p53. This work allows for

new insight into further BRCA1 studies, adding possibilities to better elucidate its structural molecular properties. Through these new insights into the 3D structure of BRCA1 it may be possible to improve rational drug design as well as begin to implement more precise, personalized medicine alternatives.

Single particle EM is an important tool for the structural study of micro and nano-sized particles such as biomolecules. In order to view high resolution images of such elusive particles, the use of electron-scale density mapping techniques is required to view the intricacies of biomolecules such as the ~250 kDa sized BRCA1 complexes. Electrons are emitted by a gun source that penetrate a frozen-hydrated silicon nitride microchip with the attached biological sample. Electrons scatter off the molecules in the specimen and are focused by a magnetic lens. The amplitudes and phases of the scattered electrons are combined to form a projection image from the central section of the sample. Images containing particles with different angular information can be mathematically combined and used to reconstruct 3D image data. In recent years, much has been done to automate the reconstruction programs, such as the development of the RELION software package (Scheres, 2012), as well as data collection processes, leaving the production of viable specimens as the remaining bottle-neck in improving high resolution cryo-EM data. The more specimens that are examined, the more biological questions can begin to be addressed.

Many aspects of the techniques used for imaging in Cryo-EM have remained largely unchanged over the past few decades. An example of this is the proliferative use of copper grids, typically carbon coated, for capturing and viewing sample in the electron microscope. Only recently have researchers and material scientists begun testing and optimizing new materials such as Silicon Nitride (SiN) for use in electron microscopy applications. These new chips make use of material properties to optimize sample capture techniques as well as enhancing imaging performance in the

microscope during electron bombardment. In addition to being more structurally reinforced than traditional grids, SiN chips offer reduced charging, no long-range diffusion, decreased sample drift due to electron irradiation, and improved defocus stability under the electron dousing experienced in electron microscopy (Dukes et al., 2013). The integrative engineering of micro-well and micro-post topographies spanning the SiN viewing membrane produces enhanced particle capture and retention during the specimen preparation steps in cryo-EM studies (Dukes et al., 2013). Partnering with Protochips Inc., we aim to change the status quo of sample preparation techniques for use in cryo-EM studies. Having discussed prospective chip designs with material science engineers at Protochips Inc. we determined the pros and cons of novel chip designs for electron microscopy applications.

BACKGROUND:

Cryo-Electron Microscopy:

Single-particle electron microscopy (EM) is a robust imaging tool developed in the 1970's, with the first image being taken in 1975 by Richard Henderson and colleagues (Jacques Dubochet, and Joachim Frank), to allow scientists to peer into the molecular structures of specimens ranging from biological to inanimate materials. The first image was taken of bacteriorhodopsin, although it was achieved at much lower resolution than what we can see today, and propelled the field of single-particle EM forward. In the year of 2017 the Nobel Prize in Chemistry was awarded to Richard Henderson, Jacques Dubochet, and Joachim Frank for their contributions in single-particle EM, further validating the use of cryo-EM to perform structural analysis on biological materials such as cells, organelles, and large proteins.

Early criticism by Ladislaus Marton addressed some of the initial problems with cryo-EM, such as the need to prevent "destruction of organic cells from intense electron bombardment" (Marton, 1934), as well as the very low contrast due to high energy electrons passing straight through the specimens (Marton, 1934). This necessity for low electron dosing intensities to study low-contrast biological samples led to the need for new sample preparation methods, with negative stain (developed in the 1940's) to be the first method used (Marton, 1934). Negative stain is a method in which biological material is coated with a thin, amorphous layer of heavy-metal salt to create a surface in which electrons are scattered more than with the biological material alone, and are more readily protected from electron damage (Hall et al., 1945; Brenner et al., 1959; Huxley et al., 1961). This coating also aids in maintaining the 3-dimensional (3D) structure of the biological material, preventing collapse due to vacuum pressure within the electron microscope (Hall et al., 1945; Brenner et al., 1959; Huxley et al., 1961).

It was determined by Aaron Klug (Nobel Prize for Chemistry in 1982) that the specimen would need to be tilted within the microscope in order to capture multiple views of the sample to ultimately achieve a 3D structure from a negatively stained specimen. Alternatively, Klug noted that the same effect could be achieved if the specimen contained a "purified" sample in which many particles could be imaged, all existing in different 2-dimensional (2D) orientations, and used to resolve a 3D structure (Klug & Finch, 1965). David DeRosier and Aaron Klug offered the first calculations for a 3D structure based on the examination of 2D projection in 1966 (DeRosier & Klug, 1968).

Exploration for freezing samples began in the 1950's as Humberto Fernández-Morán prepared thin cryo-sections for analysis using cryo-EM (Fernández-Morán, 1960). An immediate problem with Fernández-Morán's preparation method was the fact that water forms crystalline ice,

diffracting electrons, which effectively destroyed any signal originating from the sample and changed the structure of the biological specimens (Schmidt, 2006). Basile Luyet had previously noticed the problems associated with freezing biological structures in crystalline ice in the 1940's (Schmidt, 2006). At this point it was noted that samples needed to be frozen rapidly enough to avoid the formation of crystalline ice, or to introduce cryo-protectants such as sucrose or glycerol during the freezing process (Haas, 1968; Haas & Rossmann, 1970).

Kenneth Taylor and Robert Glaeser were able to produce diffraction patterns at resolutions higher than 3-Å in unprotected frozen catalase crystals, and were able to prove that hydration within the electron microscope at cryogenic temperatures could be maintained, improving contrast in comparison to the use of glucose (Taylor & Glaeser, 1974; Taylor and Glaeser, 1976). At the time, the cryo-technology was only able to produce cryo-EM studies at -120°C, which was well above what was necessary for the transition from crystalline to amorphous ice. However, due to what Taylor and Glaeser attributed to interactions among the protein surfaces and surrounding water molecules, no crystalline ice was observed in the protein crystals (Taylor & Glaeser, 1974; Taylor and Glaeser, 1976). In addition, new methodological resolutions for sample handling at cryogenic temperatures were established by Taylor and Glaeser, which showed that cooling promoted improved radiation damage resistance, making higher electron intensities or longer exposure times possible (Taylor & Glaeser, 1974; Taylor and Glaeser, 1976).

Over the subsequent decades, Henderson, Frank, and Dobochet as well as a team of other researchers improved and optimized every aspect of their cryo-EM techniques. Dobochet went on to develop an advanced, rapid freezing technique that made use of liquid ethane to counteract drying out and distortion of biomolecules when being bombarded with electrons. Henderson and others developed vastly more sensitive electron detectors, while Frank worked on the

advancement of computational algorithms that could produce commanding 3D structures through merging millions of images. In the year 1990, Dr. Henderson and colleagues reached a critical landmark in the field of cryo-EM when they showed the first high-resolution biomolecular structure via averaging techniques over many homogenous particles (Henderson et al., 1990). In this ground-breaking study, Henderson and colleagues collected data from multiple microscopes across the world in order to optimize the data quality and collection techniques (Henderson et al., 1990). Henderson claimed that detailed technical and specimen-preparation technique improvements would enable the development of cryo-EM toward a general technique: "This would then turn the technique we have been using into a routine and quick method, able to be used on many more difficult specimens, eventually including non-crystalline molecular assemblies" (Henderson et al., 1990).

Millions of Bacteriorhodopsin protein molecules in 2D crystalline orientations, allowing the total electron dose of the EM to be spread over a large number of particles, were used to achieve one of the first high-resolution structures (Henderson et al., 1990) in the cryo-EM field. Averaging particles directly in the microscope is equivalent to this analysis over a sizeable quantity of particles in 2D crystals. Averaging over asymmetrical units can be used to increase the signal to noise ratio in the case that there are non-periodic assemblies of symmetrical particles, but in general, determining positions and orientations of individual particles in images with weak signals was the greater challenge. Achieving this quantization of non-periodic assemblies of symmetrical particles would yield much better averaging techniques, but such analysis in 1990 was rendered unmanageable due to the high computational power required for such techniques (Glaeser, 1999). Henderson detailed a quantitative examination on overcoming these challenges necessary for the development of atomic-resolution (~3 Å) structures of non-crystalline molecular assemblies five

years after the initial publishing of the Bacteriorhodopsin model (Henderson, 1995). In this examination, it was established that determining the 2D position and 3D orientation of discrete particles, given particles with satisfactorily high molecular mass, would be possible through the use of low-concentration, non-caustic electron irradiation in phase-contrast EM (Henderson, 1995). Henderson's work resolved that it would be conceivable to establish atomic-resolution (~3 Å) structures from the alignment, averaging and refinement of a sensible number of particles (~10^4) given the particle of interest has a sufficiently high molecular weight (~50 kDa) (Henderson, 1995). The number and size of particles necessary for achieving atomic-resolutions structures was later revised when Glaeser offered further analysis suggesting that the size threshold of particles could be adjusted to ~20 kDa (Glaeser, 1999).

The primary issue throughout analyses of unstained, non-crystalline, asymmetrical, arbitrarily positioned particles in solution was "the alignment of features that are only faintly visible on a noisy background" (Frank, 1975). In the mid-1970's, Frank and colleagues addressed this issue by displaying a technique that used cross-correlation functions for aligning low-dose images of discrete molecules (Frank, 1975; Saxton & Frank, 1976; Frank & Al-Ali, 1975). In 1977, Frank and colleagues concluded, through quantitative analysis of negatively stained glutamine synthetase, that it would be feasible to detect arbitrarily situated particles using non-caustic electron dosages and, additionally, that it would be possible to average images of numerous radiation-sensitive particles to ultimately acquire high-resolution structures (Frank et al., 1979). In homogenous, non-crystalline specimens, determining the position (2D in the plane) and orientation (3D in the plane) consisting of five distinctive parameters remained a challenge (van Heel & Frank, 1981). In addition, biological specimens are seldom anatomically uniform and often contain impurities (van Heel & Frank, 1981; Frank & van Heel, 1982). In this wake, it became additionally required to recognize

potential anatomical sub-states to distinguish dissimilar particle types in heterogeneous specimens, as well as dissimilarities in negatively stained structures (van Heel & Frank, 1981; Frank & van Heel, 1982). In remedy to this issue, Frank and Marin van Heel developed a technique in 1981 that would allow for the assortment of particles into distinct classes based on the orientations exhibited in the images (van Heel & Frank, 1981; Frank & van Heel, 1982).

Particle images could be characterized with an n-dimensional intensity vector using n pixels where multivariate statistical analysis would then sort these vectors, appearing in clusters. A specific 2D projection of a particle with explicit orientation and anatomical properties would be represented by the corresponding cluster, for each of the clusters created. Given that particles in each cluster were assumed to be suitably alike allowed for an increase in the signal to noise ratio, improving this method for sorting images based on sensitive variances that was capable of being computationally automated. The next challenge was governing how the 2D image classes relate to each other to form the 3D counterparts for each anatomical sub-state. In 1986-1987, Frank and Michael Radermacher developed a general method known as Random Conical Tilt to examine this relationship between the 3D alignment from the classes of 2D projections of asymmetrical particles (Radermacher et al., 1986; Radermacher et al., 1987). Random Conical Tilt combined an application of tomographic conical tilt sequence, described by Radermacher (Radermacher, 1980), with the general notion of acquiring 3D information from the relative 2D projections data previously concluded under Frank and colleagues (Radermacher et al., 1986; Radermacher et al., 1987). Forming the foundation of single particle cryo-EM, Frank and colleagues were responsible for developing many of these early mathematical tools used in image analysis, assembling them into what is now known, and widely available and used among the scientific community, as SPIDER (Frank et al., 1981).

In the early stages of cryo-EM, limitations of its use for studying biomolecular anatomies associated with crystalline ice formation were anticipated to be overcome by exercising advanced cooling techniques in which liquid water could be cooled into a vitrified state (Dubochet, 2011). Prior to 1980, the concept of freezing bulk water into a vitrified, solid state was controversial at best, with theory at the time expecting the required heat transfer cooling rate to be unobtainable with known technologies. At that time, this vitrifying of water phenomena had only been validated in small volumes of condensed water vapor at cold metal surfaces (Burton & Oliver, 1935; Dowell & Rinfret, 1960). At last in 1980, the controversy of vitrifying bulk water was concluded with the demonstration that rapidly freezing micrometer-sized droplets were able to produce vitrified water, and that it may in fact be the most common form of water in the universe (Jenniskens & Blake, 1994).

In 1981, an enhanced technique for depositing a thin film of non-crystalline, vitreous, solid water on sample grids for viewing in an electron microscope was developed by Dubochet and Alasdair DcDowall (Dubochet & McDowall, 1981). Carbon coated grids mounted with sample were rapidly plunged in liquid ethane, or propane, at -190°C and preserved by further refrigeration in liquid nitrogen (Dubochet & McDowall, 1981). The slender layer of vitreous ice on the grid specimen allowed for almost constant absorption across the specimen within the cryo-electron microscope (Dubochet & McDowall, 1981). These specimens containing vitreous ice would be preserved so long as the temperature remained below -160°C as noted by Dubochet, otherwise the amorphous ice would be converted into crystalline form nearing -140°C (Dubochet et al., 1988; Adrian et al., 1984). In the years following, Dubochet and colleagues would further develop this specimen-preparation technique and would go on to demonstrate studies in pure water, DNA and purple membranes, as well as aqueous solutions of bacteriophages at cryogenic temperatures (Lepault et

al., 1983; Dubochet et al., 1982; Dubochet & Lepault et al., 1982). In 1984, the group of researchers utilized Dubochet's technique in conjunction with an enhanced cooling mechanism that allowed thin, unsupported vitrified water films to form in order to prepare and visualize micrographs of virus suspensions (Dubochet et al., 1988; Adrian et al., 1984). Maintaining arbitrarily oriented molecular complexes or whole molecules in their natural states is critically important in cryo-EM, and this enhanced cooling method developed by Dubochet and colleagues permitted for the unsupported water films to remain adequately thin for prompt vitrification, but thick enough to quarter a distinct stratum of the native state molecular complexes (Adrian et al., 1984).

By the early 1980's, Dubochet and his colleagues had finally resolved the challenges that had plagued the first 50 years of the invention of the electron microscope in cryo-EM studies: "the most abundant constituent of living things, water, has invariably been excluded" (Dubochet et al., 1985). Dubochet and colleagues had proven that their specimen preparation techniques had merit and that they could be largely applied in additional biological particle studies within cryo-EM (Dubochet et al., 1987; Dubochet et al., 1985). These new sample preparation techniques were instantly, and universally implemented by researchers in the cryo-EM field for studies involving single particle assemblies and even single object cryo-tomography.

Recent Technological Advances:

More recent developments in electron detectors, from the 1990's to 2000's until present day, have allowed for recent breakthroughs and Nobel Prize winning discoveries, creating waves in the field and across the scientific community. The newest technical developments in these sensors allow for the production of Monolithic Active Pixel Sensors, utilizing Complementary Metal Oxide Semiconductors (CMOS) technology (Faruqi et al., 2006; Milazzo et al., 2005). In the mid-2000's, utilization of these CMOS sensors for electron detection mechanisms had already begun to crop up

in reports among scientists (Faruqi et al., 2007; Xuong et al., 2004). Although, these CMOS detectors had already established merit in other fields, such as astronomy, for the study of charged particles. Later, by 2012-2013, these sensors would be referred to as Direct Electron Detectors and were extensively being used in cameras of electron microscopes (McMullan et al., 2016). Prior to these Direct Electron Detectors, Silica-based charge-coupled devices (CCD's) were being used in cryo-EM studies, but due to technical issues these devices could not be used to directly observe electrons. These CCDs required that any signal given from the flux of electrons be translated into light, automatically introducing extraneous noise into the otherwise clean signal, making film the desired choice for examining high-resolution data. However, even the new Direct Electron Detectors provided an improved signal to noise ratio over the conventional film in their capability to identify high-energy electrons at low intensities, as well the cameras' ability to operate at higher speeds than traditionally possible with film (Rubinstein & Brubaker, 2015; Ripstein & Rubinstein, 2016). With these improvements, it is even possible to record "movies" that can be used to compensate for specimen drift caused by irradiation of electrons and temperature gradients, allowing for more electron counting (Li et al., 2013; McMullan et al., 2009). The addition of innovative electron sources, like the field emission gun developed by Albert Crewe, as well as new stable cold-stages were also integral in dramatically improving the signal to noise ratio and spatial resolution in cryo-EM techniques using the Direct Electron Detectors (Li et al., 2013; Brilot et al., 2012; Campbell et al., 2012). The introduction of the Volta phase plate is another new innovation used in solving phase correction issues, encountered during defocusing steps in the electron microscope for attaining better phase contrast (Erickson & Klug, 1971; Danev et al., 2014). Advanced computational methods have also allowed for the automation of data collection in the field of cryo-EM, that has advanced the field immensely since the 1990's and inadequate computer processing

power (Suloway, 2005). These modern developments in image-processing and advanced programming such as 'likelihood algorithms' have become essential to the field when superior resolution data was finally realized using the newest electron detectors (Sigworth 1998; Scheres et al., 2006).

In a Nutshell:

Over half a century has passed since John Kendrew's and Max Perutz's Nobel Prize winning work on myoglobin and hemoglobin for their studies of globular proteins' structures. Over four decades have passed since the high-resolution construction of hemoglobin in liquid solution was depicted using cryo-EM, setting the foundation necessary for the advancement of the field (Khoshouei et al., 2017). Utilizing cryo-EM techniques in 1990, the first high-resolution (~3 Å) structure was achieved. Another ten years passed before high-resolution images of icosahedral and helical particles were achieved using data chronicled on traditional film. Once the Direct Electron Detectors were introduced, yet another decade later in 2012-2013, and early accounts of de novo atomic structural representations of small distinct particles such as $TRPV_1$ (Transient Receptor Potential Cation Channel Subfamily V Member 1, a membrane protein ion channel) were produced, cryo-EM has promptly become imperative to the field of structural biology (Liao et al., 2013). Laureates Jacques Dubochet, Joachim Frank, and Richard Henderson provided major contributions, without which the field of cryo-EM would not have developed into the captivating state in which it exists today (Oikonomou & Jensen, 2017; Rubinstein, 2017). Dubochet established specimen preparation techniques for the analysis of biomolecules in water using cryo-EM (Fischer et al., 2010). Frank established techniques using analyses of clusters of particles in solution for defining structural data of biomolecules (Hite & MacKinnon, 2017). Finally, Henderson validated the prospect of utilizing cryo-EM to attain atomic resolution structures of biomolecules (Zhao et

al., 2015; Dashti et al., 2017). All of these advancements, when utilized in cryo-EM, can provide data that may yield functional information about biomolecules, such as monitoring structural changes or defining free-energy sites, that have remained elusive to scientists to date (Dashti et al., 2014; Kühlbrandt, 2014).

Silicon Nitride Microchips vs. Traditional EM Grids:

Advances in the material science include the production of graphene (Yuk et al., 2012), and Silicon Nitride (SiN) membranes that can serve as novel substrates for liquid compartments in Transmission Electron Microscopy (TEM) imaging (Ring & de Jonge, 2010; Klein et al., 2011). The use of these SiN microchips in TEM applications is vastly appealing due to their durability over the fragile, traditional holey carbon grids, as well as their manufacturing and flatness consistencies in the nanometer thin membranes (Tanner et al, 2013). SiN microchips, such as the Poseidon system (Protochips Inc., Raleigh, NC, USA), allow for the capture and viewing of macromolecules in solution within the TEM in a precise fashion (Degen et al., 2012; Gilmore et al., 2013). Distinct regions of the SiN imaging membrane can be incised down to produce 50 nanometer (nm) thick micro-wells, or to produce a spanning area of 50 nm thick film with 150 nm posts remaining across the imaging plane for improved sample detention. These features contribute to uniform arrays of either micro-wells or mico-posts that can accommodate 150 nm of liquid or frozen layers. **Figure 1** displays in more detail the layout and the features of the silicon nitride microchip described previously. The SiN microchips, with incorporated microwell and micropost arrays, provide a unique advantage over traditional substrates in that the 200 nm thick membranes aid in reducing bulging effects while inside the vacuum of the TEM (Vlaasak & Nix, 1992). The microwell and micropost arrays that are only 50 nm thick at the base of the substrate provide an additional 150 nm that can allow sufficient solution depth for imaging near native-state biological complexes (**Figure 1 A,B**). These arrays

permit thin sections of frozen-hydrated or fully liquid specimen layers to be formed for the visualization of biomolecules in cryo-EM on the SiN microchips.

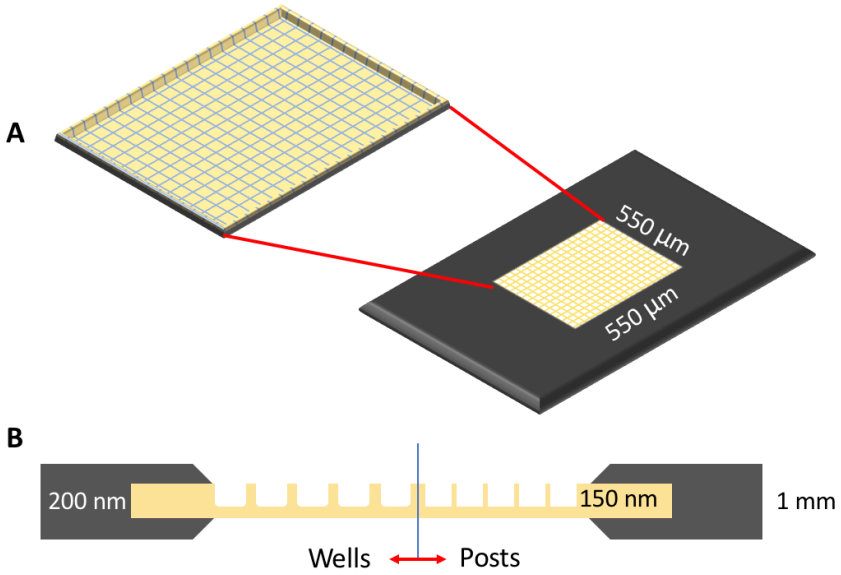

Figure 1: Silicon Nitride (SiN) Microchip specifications with microwell or micropost arrays integrated on the viewing window surface. (A) SiN microchip with 5 x 5 x 1-mm frame dimensions exhibits a thin (50 nm thick) TEM viewing window of dimensions 550 x 550-µm with integrated microwell or micropost arrays. Originally 200 nm thick, select regions (wells or area around posts) have been etched down to 50 nm leaving 150 nm for liquid depth. **(B)** Side view of SiN microchip with a viewing window composed of a 200-nm thick SiN membrane comprised of microwells (~10 x 10 µm) or microposts (~20 x 20 µm spacing) that can accommodate a liquid layer of 150 nm thick in the path of the electron beam within the TEM.

These microchips have been employed in past studies for visualizing processes relating magnetic resonance imaging (MRI) contrast, micelle suspensions, liposome drug delivery systems, and transcriptionally active rotavirus double-layered particles (DLP's) in real-time (Dukes et al, 2013). The array of such micro-wells or micro-posts can be varied through engineering processes to produce different chip-specimen properties, tailorable to particle size and imaging requirements. As SiN microchips are hydrophobic in nature, they provide an ideal substrate to promote interactions with the lipid tail groups that are exposed at the air-water interface in the

Nickel-Nitrilotriacetic Acid (Ni-NTA) lipid layers. An additional advantage observed with SiN chips is that the 200 nm thick membranes aid in minimizing protrusion of the viewing windows when exposed to the TEM vacuum system (Vlassak & Nix, 1992). In 2012 a study was produced in which E. A. Ring and colleagues utilized SiN microchips, and their robust engineering design, to culture cellular samples directly on the membranes and combined two chips to produce an improvised microfluidic chamber for imagining liquid specimen (Ring & Dukes et al, 2011). In addition, reproducibly thin, ice-layered specimens have been reliably produced using SiN microchips under mild blotting techniques for applications including rotavirus complexes in active transcriptional processes (Tanner et al, 2013).

Using SiN microchips in cryo-EM, dubbed Cryo-SiN, has been shown to exhibit enhanced image contrast over conventional holey carbon or other traditional sample grids under identical preparation procedures and imaging conditions (Tanner et al, 2013). Improved contrast correlates to more accurate 3D data that in turn yields less expensive 3D reconstruction calculations, producing superior 3D structures with less required images (Tanner et al, 2013). Due to the difficulty in manufacturing uniformly flat, and durably robust holey carbon film, the traditional grids exhibit charging-effect limitations produced via beam-induced movement (Tanner et al, 2013). Generally, techniques such as the addition of amorphous carbon layers to blanket the perforated film are employed to mitigate the charging effects, which become obsolete through the utilization of cryo-SiN (Tanner et al, 2013). Holey carbon grids have been in use for the past half-century, and only recently have more robust, novel support films with conductive properties, commonly used in the semiconductor industry, been in development. As the production of carbon support films can be highly variable, surfaces that are invariably flat, impermeable, and transparent to the electron beam would provide a valuable tool to the EM community. These new support

films, such as titanium-silicon metal glass, silicon carbide, and the newer ultrathin silicon and silicon nitride films, were developed in an effort to reduce electron-beam related movement and charging-effects while imaging frozen-hydrated samples (Tanner et al, 2013; Rhinow et al., 2008; Yoshioka et al., 2010). Near-atomic resolution specimens, including graphene (Brown et al., 2012), nanoparticles (Chen et al., 2013), and unstained DNA origami complexes, have been achieved through the use of cryo-SiN techniques in recent years (Tanner et al, 2013). In fact, the first achieved, atomic-resolution tomogram of unstained nanoparticle sample can be attributed to advanced silicon membranes (Yuk et al., 2012; Scott et al., 2012). Additionally, some of the only atomic-level 3D tomographic data collected have been provided through tilt-series at steep angles (±83°) on SiN membranes (Yuk et al., 2012; Scott et al., 2012). When comparing frozen hydrated biological specimens prepared on holey carbon films to cryo-SiN membranes, we noted key differences in the recorded images and downstream computational analyses. When recording EM data, ensuring accurate alignment between image frames, necessitates the use of extremely flat specimen substrates and no drift conditions to achieve suitable tomographic reconstructions. Achieving such results advocate that SiN membranes possess uniform flatness superior to traditionally used carbon substrates (Tanner et al, 2013).

Tanner and colleagues previously provided work to demonstrate the feasibility of isolating various, distinct negatively stained and frozen-hydrated specimen on carbon-based substrates for EM (Kelly et al., 2008; Degen et al., 2012). Following this work, Tanner and colleagues also assessed negatively stained rotavirus DLP specimens using SiN microchips (Gilmore & Tanner et al., 2013). In continuation, the next logical step involved investigating actively transcribing DLP's for cryo-EM using the novel SiN microchips for further verification of the quality of the membranes to traditional grids (Tanner et al., 2013). The rotavirus DLP's in this study were abundantly captured in their

active state using the SiN microchips before being vitrified and visualized through single particle cryo-EM (Kam et al., 2014). As described in previous work, specimen preparation and incubation reactions were efficiently accommodated directly on the SiN microchips in advent to plunge-freezing processes (Gilmore & Tanner et al., 2013). With traditional holey carbon grids serving as a suitable control for consistent use of reagents and preparation techniques, it was determined that cryo-SiN offered enhanced visual contrast reportedly due to a potential decrease in adverse charging-effects as well as the aptitude for SiN specimens to achieve thinner, more precise frozen-hydrated sample layers under identical preparation and imaging conditions (Tanner et al, 2013).

Previous work also resolved a higher resolution view of capsid layer structures of inactive, frozen-hydrated rotavirus DLP's that remain consistent with the work produced by Tanner and colleagues, featuring similar to identical external capsid architectures (Kam et al., 2014). However, through the utilization of cryo-SiN techniques and their purported image contrast advantages, unique and strongly-defined internal capsid layer density features were discovered that had previously been lacking in the holey carbon specimen 3D reconstructions (Tanner et al., 2013; Zhang et al., 2008). The internal core densities of these actively transcribing DLP structures had been under-defined and relatively absent in previous studies, consistent with Tanner and colleagues' findings when using holey carbon film (Lawton et al., 1997). These differences suggested that cryo-SiN did, in fact, offer a superior visual contrast among every individual particle, which serves to decrease the necessary computation among particle selection, alignment, and reconstruction routines in the SPIDER and RELION software packages. Given the enhanced differences exhibited by cryo-SiN technology, it could now be possible to calculate 3D structures of biological molecules, such as DLP's, using just a small portion of the number of images and particle counts typically required using traditional holey carbon specimens (Tanner et al, 2013). However,

it was yet to be demonstrated whether or not cryo-SiN technology held similar advantages when using biological assemblies lacking icosahedral symmetry, such as the case of BRCA1.

Furthermore, the findings the Kelly Lab suggest that silicon-based membrane surfaces offer higher versatility in viewing fundamental viral assembly processes. All of this data, with improved information through the use of cryo-SiN, foster virologists', and other fields of biological science, the ability to study biological mechanisms in an improved, entirely new light. Cryo-SiN technology, thus far, has allowed researchers to achieve thrilling results that could hold huge potential in unstained structural biology specimen preparation procedures of the future. Ergo, cryo-EM studies employing the use of SiN substrates may be able to provide distinctive new insights into biomolecular processes and aid in the development of enhanced therapies in fields including, but not limited to, antiretroviral vaccines, personalized cancer medical interventions, and much more, to preserve and improve human life. The utilization of SiN microchips for novel TEM substrates for viewing biological samples is particularly valuable for correlative-light microscopy (LM) and for EM (Peckys et al., 2010a), where LM can be used to see lower-resolution data to identify areas of interest, and EM is used to 'zoom' in on a sector of significance to attain nanometer resolution (Gaietta et al., 2002). All signs of Tanner and colleague's work pointed to the highly awaited use of SiN microchips for investigating vital life-cycle processes of protein assemblies in native-resembling conditions.

METHODS:

Protein Extraction and Sample Preparation of BRCA1 Assemblies:

The MDA-MB-361 line of human adenocarcinoma breast cancer cells (ATCC) were grown to approximately 80% confluency in a 5% CO_2, 37°C environment using RPMI-1640 culture medium

(Mediatech, Manassas, VA, USA) with the addition of 20% Fetal Bovine Serum (Fisher Scientific, Hanover Park, IL, USA) and 0.5x Penicillin Streptomycin (Fisher Scientific, Hanover Park, IL, USA). Once cells were amassed into pellets after detaching them with trypsin-EDTA (Life Technologies, Carlsbad, CA, USA), they were then centrifuged at 500g for 5 minutes followed by a wash with phosphate-buffered saline (PBS). Post wash, the MDA-MB-361 cell pellets were lysed using the NE-PER extraction kit (Thermo Scientific, Miami, OK, USA) and the nuclear contents were collected for further enrichment. Diluting the contents to ~1 mg/ml with HEPES buffer (20 mmol/l HEPES, 2 mmol/l $MgCl_2$, pH 7.2) including 5 mmol/l imidazole as well as protease inhibitor cocktail (EDTA-free, Roche, Branchburg, NJ, USA), the extracts were then incubated with equilibrated Ni-NTA agarose beads (Qiagen, Hilden, Germany) to enrich for BRCA1 complexes (**Figure 2B**). Incubation lasted 1 hour on a medical rotator in a 4°C cold room where the solution was then added to the Nickel-NTA beads. The flow-through material was captured and stored for further analysis. Following three washes of the Nickel-NTA beads with HEPES buffer accompanied with 140 mmol/l NaCl and 5 mmol/l imidazole, multiple, subsequent eluates were captured and stored for further analysis using HEPES buffer with an increased 150 mmol/l imidazole. Bradford Assays were employed for estimating protein concentration in the remaining, stored eluates and flow through samples. Eluate number 3 (E3) was determined to be the most enriched for BRCA1 (0.241 μg/μl), and was prepared with a concentration of 0.05 μg/μl for further cryo-SiN study.

Lipid monolayers comprised of 25% functional Ni-NTA (Avanti Polar Lipids, Alabaster, AL, USA) were placed over 15-μl aliquots of purified (Milli-Q) water on parafilm, sealed and incubated within a petri dish for one hour. The SiN microchips were placed on the 25% Ni-NTA monolayers with the viewing membrane face down for one minute incubation periods. Once incubated on the lipid monolayer (**Figure 2A**), the SiN specimen was carefully removed and transferred to forceps

specific to the VITROBOT blotting and plunge freezing apparatus (FEI Company). Once secured in these forceps, a Hamilton Syringe and blotting paper were used to gently remove the excess fluid from the incubated lipid monolayer in preparation for sample deposition.

The surface of the SiN microchip was blotted to remove the excess liquid from the monolayer application. Aliquots of enriched E3 sample (3 µl each) were added to the surface of the chip for 1 minute, while ensuring the sample completely covered the viewing film. After sample incubation, the specimen was then transferred to the VITROBOT plunge freezing device (FEI Company) using the specialized forceps. The VITROBOT computer program was set to blot for 5-10 seconds across each of multiple SiN specimens. The specimens were blotted and directly plunge-frozen in liquid ethane at roughly -190°C to develop the vitreous ice necessary for cryo-EM. The cryo-SiN specimens were then quickly transferred from the liquid ethane to liquid nitrogen for preservation and further study.

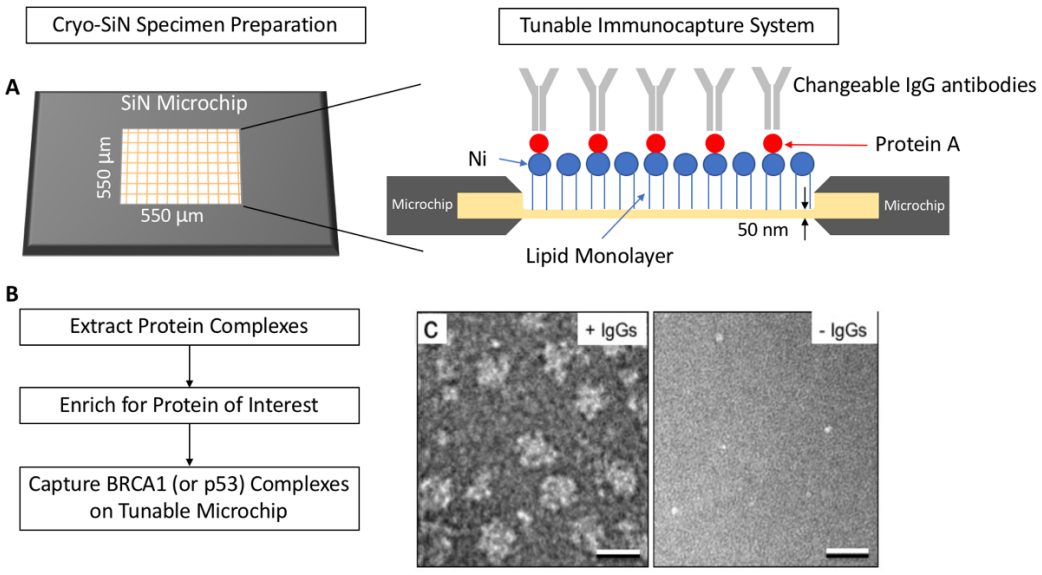

Figure 2: Tunable SiN microchips used to capture and view protein complexes such as BRCA1 or p53, as well as other biomedically relevant assemblies. (A) Graphic representation of the tunable, interchangeable layers applied to the SiN microchip surface that include a lipid coating (blue),

protein A (red) and changeable antibodies (grey). **(B)** Flow chart displaying the specimen preparation procedures using the tunable SiN microchip technique. **(C)** Representative images of BRCA1-RNAP II complexes with (+IgGs) and without antibodies (-IgGs) presented in previous work by the Kelly Lab (Gilmore et al., 2015). Scale bar is 20 nm.

When cryo-EM specimens are negatively stained the biological particle environment naturally becomes dehydrated, essentially eliminating some features of their native, structural integrity. Producing an immobilized, frozen-hydrated environment through cryo-EM allows for the preservation of a near-native aqueous environment while also diminishing radiation damage to the sample under electron firing conditions in the TEM (Baker & Rubinstein, 2010). Sample freezing takes place at a rate of -10^6 °C/s in order to achieve vitrified ice (Dubochet et al., 1988). In the case that the freezing process occurs too slowly, or if the temperature of the specimen is warmed above about -140°C, then the vitrified ice will start to devitrify back into a crystalline state (Dubochet et al., 1988). Crystalline ice conflicts with TEM imaging processes via electron diffraction as well as corrupting the biological sample by removing water molecules from the hydration sheathing of the specimen. Humidity controlled conditions are exceedingly important to cryo-EM studies in an effort to reduce any ice or specimen contamination.

Cryo-Electron Microscopy:

The cryo-SiN specimens were transferred from liquid nitrogen preservation to the Gatan Single Tilt Liquid Nitrogen Cryo Transfer Holder (Model 626, Gatan, Inc., Pleasanton, CA, USA). The Gatan Transfer Holder had previously been pumped down to ~5 x 10^{-6} Torr using the Gatan Turbo Pumping Station (Model 655, Gatan, Inc., Pleasanton, CA, USA) to ensure adequate vacuum pressure for cryo-EM. Once the dewer and tip of the holder had sufficiently cooled (~ -200°C), the Gatan Transfer Holder was then transferred into a FEI Spirit BioTwin Transmission Electron Microscope (FEI Company). The TEM is equipped with a LaB_6 filament, operating at 120 kV under low-dose conditions (5-10 electrons per $Å^2$) for imaging of cryo-SiN specimens. One-hundred

images with a pixel-size of 30-μm at 50,000x magnification (generally used for Wild-Type BRCA1 complexes) were recorded with a FEI Eagle 2k HS CCD camera (FEI Company) for a 6 Å per pixel sample volume. An additional fifty images were taken with a pixel-size of 30-μm at 68,000x magnification (generally used for mutant complexes) with the same CCD camera mentioned previously at a 4.4 Å per pixel sample volume for further analysis. From the initial 100 images taken at 50,000x magnification, 5401 particles were manually selected using the SPIDER software package.

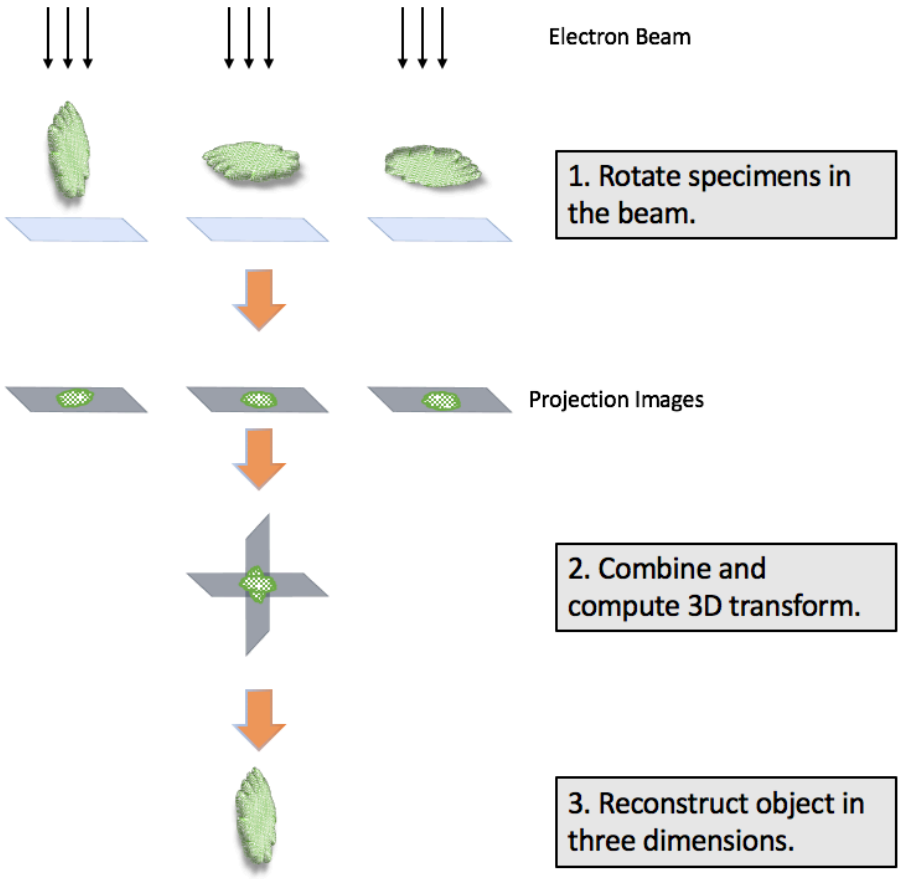

Figure 3: Schematic of TEM processes for achieving 3D structures from 2D Images. (1) Particles captured on the tunable SiN microchip system in different orientations for image acquisition. **(2)** These differently oriented particles can be combined to compute 3D transform data either via tilting the specimen in the beam, or simply by combining random sampling of orientations. **(3)** The 3D data is then reconstructed to reveal the 3D structure of the particles of interest.

Image Processing and 3D Reconstruction:

The SPIDER software package was used for processing of the 100 images and 5401 selected particles. Multiple scripts developed by Dr. Kelly and colleagues were used to select particles in SPIDER, generate good particle files after separating out bad particles (featureless blobs, two particles touching, etc.), developing class averages from alike particles, and creating image stacks for similar classes to be used in specific structural reconstructions. From the 5401 'good' particles, separate stacks were created based on the 20 classes generated via the culling process in the SPIDER protocol. One stack was labeled for BRCA1, another for p53, one for burst protein complexes known as air-water interface particles (referred to as AWIPs in the Kelly lab), and another for unknown class averages too small to be either BRCA1-BARD1 assemblies or p53. Of the 5401 particles, ~1600 were used in the BRCA1 stack for further 3D processing in the RELION software package. The 3D reconstruction and refinement procedures were carried out in the RELION software package utilizing an initial model of BRCA1 from previous work done at the Kelly lab (Liang et al., 2017). This original model was referenced in the initial steps of refinement to aid in allocating alignment parameters to each particle, where later iterations relied strictly on the collected experimental data by setting the regularization parameter in RELION to T=4 (T=1 represents no model bias, T=10 represents full model bias). A 3D structure of BRCA1-BARD1 complexes was masked at ~250 Å while following customary reconstruction procedures. Additionally, a 3D structure of a p53, being the first ever presented from native cellular sources, was also determined using a ~100 Å mask while implementing the same RELION processing steps applied to the p53 stack mentioned previously. RELION output eight distinct structures for both BRCA1 and p53. These reconstructions are independent of the pre-defined initial parameters representing Bayesian statistical comparisons between the experimental micrographs and the

provided initial model. **Figure 4** shows these data collection and refinement processes in a more detailed, step-wise fashion.

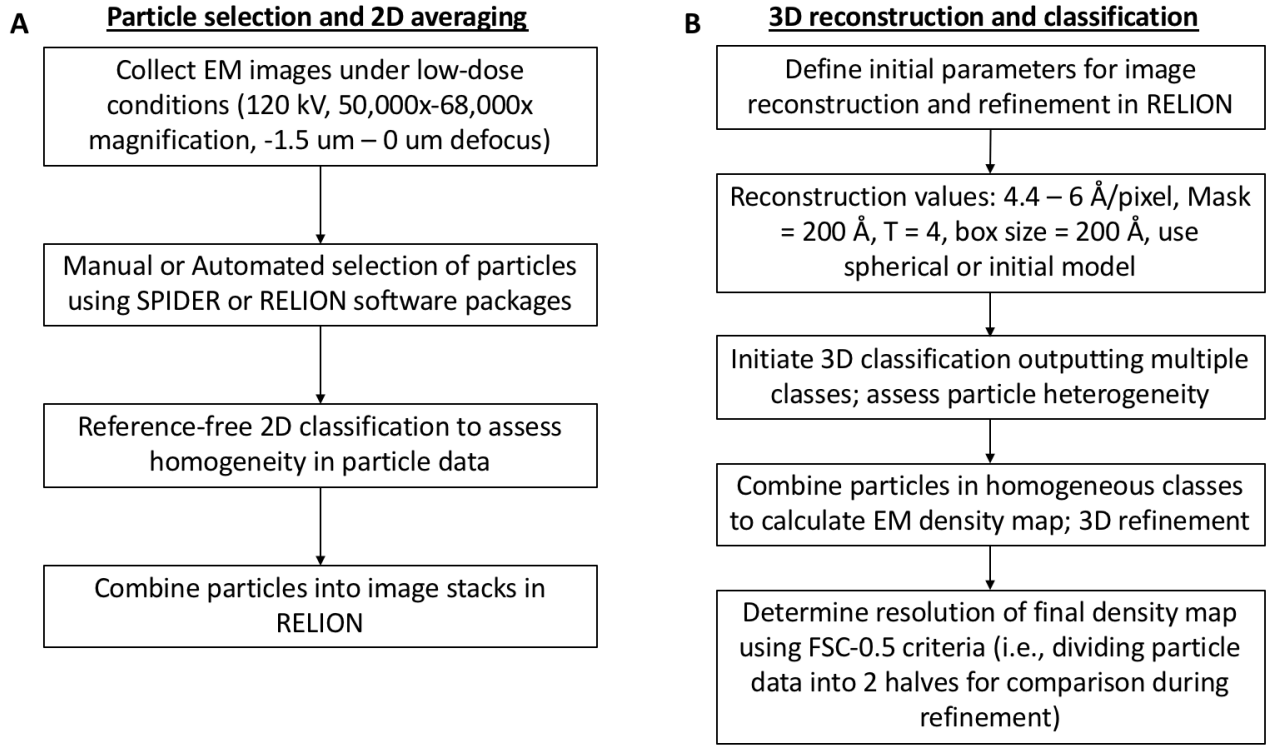

Figure 4: Flow chart for the image processing protocol used for each EM reconstruction, exhibiting a strategy for overseeing particle heterogeneity. A) Particle classification procedure for 2D averaging in either the SPIDER or RELION software packages. **(B)** Particle classification for 3D refinement procedures in the RELION software package. Managing particle heterogeneity for flexible structures can be better achieved through the supervision of the computing outputs at each iterative step in the process. The recently published work in *Science Advances* (Liang et al., 2017) by the Kelly Lab presents successful implementation of this strategy.

Molecular Modeling:

The Chimera software package (Petterson et al., 2004) was used to visualize the protein reconstructions in this study. Chimera employs energy minimization techniques for determining optimum density and model fit for verification of structure integrity (Winton et al., 2016). These energy minimization strategies apply algorithms for force calculations generated by different atomic model orientations while simultaneously evaluating atom positions requiring the least

amount of force (Winton et al., 2016). Chimera searches for a local minimum without trying to find a global minimum or overstepping energy barriers. Iterative optimization techniques can be calculated on each atom in the model to achieve the orientation for the model at the local minimum (Winton et al., 2016). A force limit can be set such that the iterative atom-moving process is repeated until forces fall below this limit and are minimized (Winton et al., 2016). Chimera can also perform masking techniques that allow for the reduction of noise in a given 3D model produced via RELION processes (Winton et al., 2016). Chimera allows the user to visualize cross-sections through a 3D density map to assess its internal contents (Winton et al., 2016). These techniques are highly relevant in biochemical applications as natural atomic arrangements in biomolecules typically arrange in ways to minimize these forces, correlating to the most likely configuration for the models in Chimera.

RESULTS:

Colorimetric Quantification of BRCA1 through ELISA:

Preliminary work, prior to the capture and imaging of BRCA1 complexes, involved the colorimetric detection and quantification of BRCA1. To achieve this, ELISA protocols tailored to the capturing of BRCA1 complexes in the Kelly lab were developed, which can be seen in **Appendix A**. An ELISA (enzyme-linked immunosorbent assay) is an experimental protocol in which the use of relevant antibodies and a color-active reagent are used to capture a specified antigen, in this case BRCA1, and detect/quantify the concentrations of the antigen respectively. The specific ELISA that was developed is known as the Capture Assay or “sandwich” ELISA. This “sandwich” ELISA utilizes various antibodies, the antigen, and color-active substrate to ultimately detect antigen concentration levels.

In brief, one first binds the capture antibody to a 96-well microtiter plate, then sample or antigen is applied that binds with the initial antibody, followed by the addition of primary antibody to bind to the unbound side of the antigen, which then houses a second antibody-enzyme conjugate. A specific enzyme is allowed to react with the substrate or reagent to produce color. This combination of antibodies and sample binds together to form a pillar extending from the base of the microtiter plate, in which the antibodies have been tailored to react with the specific sample one is hoping to capture and measure. Once the colorimetric reagent reaction has taken place one can simply use a 96-well plate reader to record the findings. In **Appendix A**, one can see the optimization process, the aims of the protocol, as well as the actual ELISA protocols that were developed. Two distinct protocols were developed that exhibit slight differences in the necessary materials as well as changes in the "capture" and "primary" binding steps. The objective of these ELISA protocols is to determine the affinity of BRCA1 binding capability as well as the affinity of BRCA1-RNA Polymerase II (BRCA1-RNAPII) in multiple testing scenarios, such as application of oxidative stress as well as testing with natural and mutant forms of BRCA1, ubiquitinated and ubiquitin cleaved BRCA1, and how these various forms interact with its main binding partners such as BARD1, and p53, etc.

Optimization procedures were also developed for the use of these protocols. A one variable at a time (OVAT) approach could be used to first optimize the capture antibody. Different levels of capture antibody, from low concentration to high concentration, could be tested on a 96-well microtiter plate in conjunction with the rest of the ELISA protocol where saturating levels of antigen are used as well as ample levels of primary and secondary antibodies so that these variables do not operate as limiting factors in the optimization of the capture antibody. Once a concentration of capture antibody is seen to provide optimal signal with low levels of noise, and the use of a higher

concentration produces little to no increase in signal, one would have determined the optimal concentration of capture antibody. One then repeats this process for the primary antibody as well as the secondary antibody in order to determine optimal concentrations to use for each of the antibodies in the ELISA protocol.

A much more robust optimization tactic, known as multiple variable at a time or multi-variable optimization (MVO), could also be used to determine the best combination of antibody concentrations to use as well as where one would see the interactions exhibited between the different variables in an experimental design. The process could be set up by determining a low, medium, and high concentration of each of the antibodies to be optimized where each possible combination would then be tested to determine which gives the optimal signal to noise ratio. If higher precision is desired, one could carry out this process multiple times, each time setting up "low, medium, and high" concentration levels that are closer to the optimal concentration determined in the previous iterations.

In this experiment, the MVO approach could be taken in conjunction with the OVAT approach in order to optimize the concentrations to use for the various antibodies and antigen respectively. The OVAT approach helped to determine the optimal concentrations of antigen sample to use by selecting manufacturer suggested concentrations of antibodies (concentrations that also correspond well in similar types of experimental use) and holding those constant while simultaneously varying the concentration of antigen from low dilutions to high dilutions [rows G and H on 96-well microtiter plates]. The optimal sample concentration was determined by selecting the dilution in which addition of more sample no longer noticeably increased the signal to noise ratio (or the point in which the signal begins to level off). Once the optimal sample dilution was determined, this amount would then be used in the further optimization of the antibodies

themselves for better signal to noise ratios using the MVO approach previously described. The plate setup can be seen in **Table A1** and **Table A2** in **Appendix A** for the design of this optimization process.

Negative Stain Reconstruction of MDA-MB-361:

To complement biochemical analysis of BRCA1 assemblies, 3D reconstructions were performed. We first used negatively stained specimens on traditional carbon-coated copper grids to serve as both a screening tool and as an appropriate control for further cryo-SiN work. In this preliminary work, MDA-MB-361 cells were cultured and enriched for BRCA1-BARD1 complexes using techniques described earlier (Please see the Methods, MDA-MB-361 BRCA1 Extraction and Sample Preparation section). Antibodies raised against BRCA1 were used to tether the enriched complexes to the surface of the microchips, and while IgG antibodies can potentially bind at two separate sites the preliminary data did not show any particle overlap that would provide a hindrance to further particle extraction procedures (**Figure 5A**). Co-IP investigations and SDS-PAGE and western blot evaluation on BRCA1 confirmed the presence of BRCA1 (~250 kDa) and BARD1 (~87 kDa) and their association as well as the presence of p53 (~53 kDa). An FEI Spirit BioTwin TEM functioning under low-dose conditions at 120 kV, outfitted with an FEI Eagle CCD camera was used to collect images from negatively stained EM specimens containing isolated BRCA1 and p53 complexes.

Discrete complexes were selected from the images using ordinary reference-free alignment procedures in the SPIDER software package to calculate class averages (**Figure 5A**). These class averages were then used for further refinement in the 3D classification procedures of the RELION software package (Scheres, 2012). BRCA1-BARD1 structures were calculated and particle heterogeneity was visually assessed (**Figure 5A B**). The data was separated into three equal-part

classes with roughly 33% of the particle data being assigned to each class. The similarity between the 3D structures output by RELION, using these three classes of evenly distributed particles, suggested that there was highly homogeneous particle data and also supports the claim that BRCA1-BARD1 complexes are decidedly not as flexible in their dimeric form. RELION did not output any additional classes, which would also suggest homogeneous data. The most intriguing finding from these negative stain reconstructions of MDA-MB-361 BRCA1 complexes is an enlarged C-terminal region calculated using the metastatic cell line, not found in the reconstructions from other cell sources, with all other biochemical information remaining consistent with that of primary cancer cells. In light of these findings, it was expected that modifications or other bound substances were responsible for the extra density in the C-terminal region of these specific proteins, and that these changes would show up again through further cryo-EM analysis.

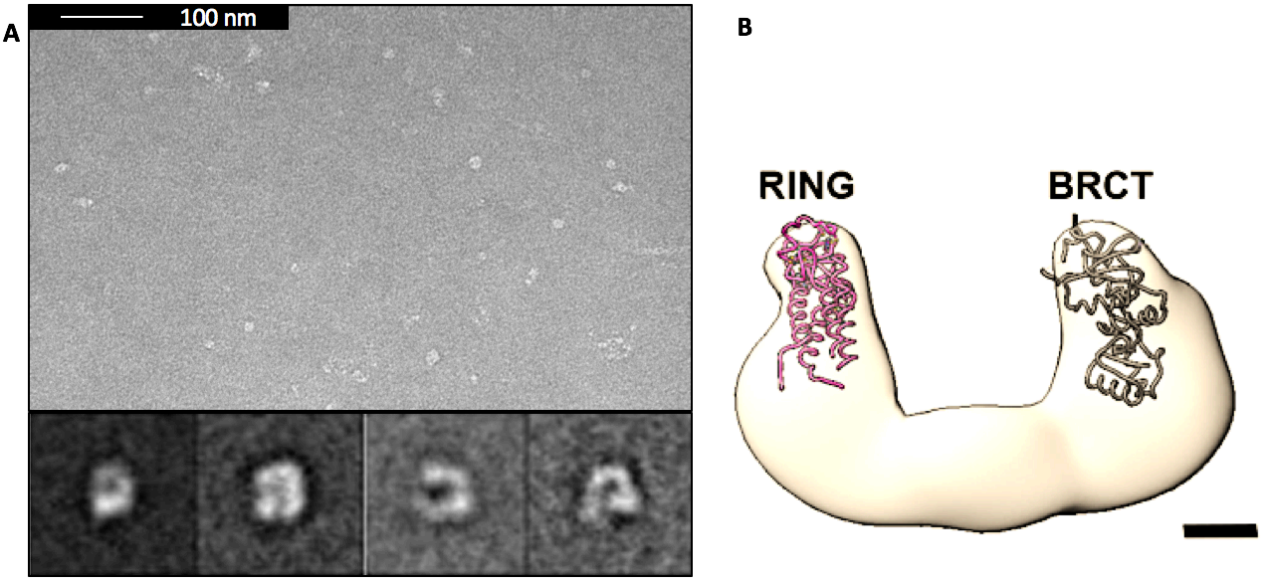

Figure 5: Preliminary analysis of BRCA1-BARD1 complexes derived from metastatic cancer cells. **(A)** Representative EM image and 2D class averages of BRCA1-BARD1 complexes from metastatic human breast cancer cells. Scale bar is 100 nm. **(B)** Atomic models of the RING and BRCT domains, (pdb code, 1JM7; Brzovic et al., 2001) and (pdb code, 1JNX; Williams & Green, 2001) respectively, fit within the EM density maps produced using standard RELION routines. Scale bar is 2 nm.

Antibody labeling analysis was used to differentiate the BRCA1-BARD1 N-terminal RING domain (Brzovic et al., 2001) from the C-terminal BRCT domain (Williams & Green, 2001), in which the insertion of atomic models (pdb code, 1JM7; Brzovic et al., 2001) and (pdb code, 1JNX; Williams & Green, 2001) respectively allowed us to interpret the 3D density map (**Figure 5B**) (Gilmore et al., 2015). A Fourier Shell Correlation (FSC) of 0.5 was used to conclude that the angular distribution among the particles were unrestricted in alignment parameters, and that a structural resolution of ~14.5 Å was achieved. Phosphorylated BRCA1 (~260 kDa) was revealed to interact with BARD1 (~87 kDa) through western blot analysis of co-immunoprecipitation (co-IP) and SDS-PAGE, and additionally indicated the presence of p53 (~43 kDa).

Proof-of-Concept Postchip MDA-MB-361 Reconstruction:

In addition to the initial negative stain work discussed previously, cryo-SiN was also employed in various testing conditions to optimize specimen preparation techniques, in which an initial 3D reconstruction of frozen-hydrated BRCA1 specimen from an MDA-MB-361 cell line was achieved on a post-array SiN microchip (Protochips Inc). Using the FEI Spirit BioTwin using similar procedures discussed in the section Negative Stain Reconstruction of MDA-MB-361, 12 images were collected from a cryo-SiN specimen at 68,000x magnification to yield a final particle count of ~200 particles. These particles were used to develop a single 3D reconstruction of a BRCA1-BARD1 complex exhibiting a 'C-shaped' clamp-like structure with a diameter of ~120 Å as described previously, with some enlargement in the C-terminal domain. The data collected from this sample was biochemically consistent with work that was previously published in *Science Advances* (Liang et al., 2017) by the Kelly lab using the same cell line, in which a flexible core region and no enlargements to either the N-terminal or C-terminal regions was displayed. During this preliminary, proof-of-concept cryo-SiN work ~200 particles were collected from 12 images and were used to calculate

representative 2D class averages for BRCA1-BARD1 complexes (**Figure 6A**). These 2D averages were then fed into the standard RELION routines to develop the 3D data necessary for building the 3D structure. Standard Chimera software package procedures were used to assess the 3D density map from the data created in RELION to achieve a 3D reconstruction (**Figure 6B**) using cryo-SiN, that remained consistent with previous work in the Kelly lab. This data provided the foundation for further cryo-SiN analysis of protein complexes formed in metastatic cancer cells.

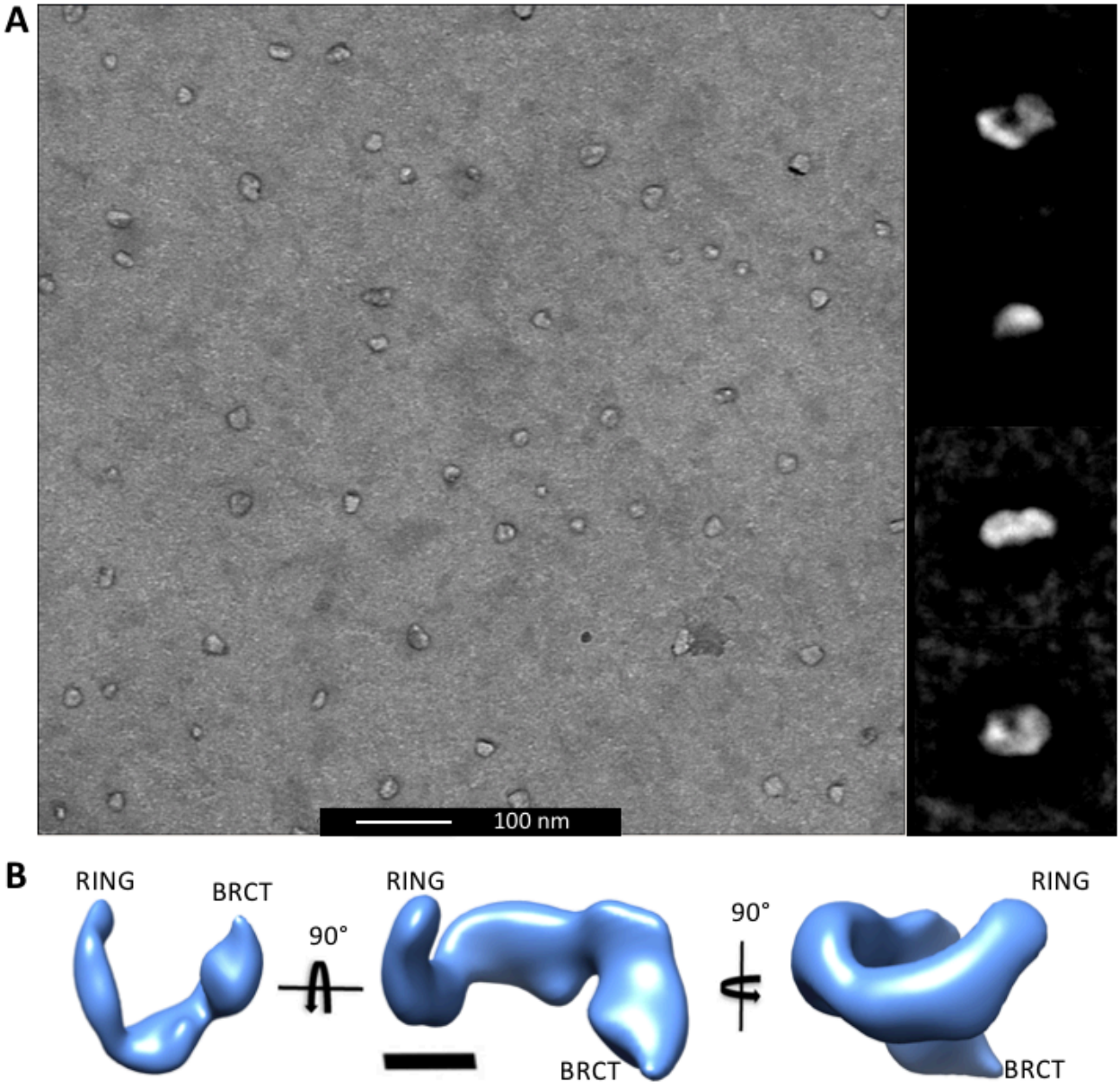

Figure 6: Primary investigation of wild-type BRCA1-BARD1 complexes derived from MDA-MB-361 cancer cells. A) Representative EM image and 2D class averages of BRCA1-BARD1 complexes from metastatic human breast cancer cells. Scale bar is 100 nm. **(B)** 3D density maps of BRCA1-BARD1 structure with labeled RING and BRCT domains achieved through standard RELION routines and visualized in the Chimera software package. Scale bar is 2 nm.

We again utilized the FEI Spirit BioTwin (FEI Company) to collect 100 images at 50,000x maginification. The images contained 5401 particles that were selected and statistically classified into discrete imaging stacks based on particle size and their defined contrast features. Of the total data, ~1600 particles comprised the BRCA1 complexes image stack, and ~1600 particles comprised the p53 classification. The remaining particles were attributed to air-water interface particles, also defined by the Kelly lab as AWIPS, and an additional stack of particles that were believed to be too small. Of the ~1600 particles associated with the BRCA1-BARD1 stack, RELION was used to process and produce eight separate, equally divided classes of approximately 200 particles each. Of these eight structures output by RELION, particle and class homogeneity remained high amongst the data presented in **Figure7**, resembling the structure shown in **Figure 6**. The particle homogeneity among the eight initial p53 structures output by RELION were also markedly high, with p53 forming a tetrameric structure. The single p53 reconstruction, after combining the eight output classes, is displayed in **Figure 8**. The 3D structures achieved in this work were taken from the enhanced particle capture of the cryo-SiN technology on a micro-well chip designed by Protochips Inc. This particular chip design lacked posts but contained 5 μm well-lines across the whole surface of the chip. The chip was engineering with 15 μm spacing between lines, and a 550 μm by 200 μm window. Other samples were frozen on a similar chip with a larger imaging window (550 μm by 550 μm), as well as multiple post-chips with similar respective window sizes for reproducibility. Initial data that led to the 3D reconstruction in the Proof-of-Concept Postchip MDA-MB-361

Reconstruction section was achieved using one of these post-array SiN microchips (550 μm by 550 μm window, pillars on the whole surface of chip, 5 μm pillars, 20 μm spacing). These features are easily distinguished in the FEI Spirit BioTwin electron microscope, where fiducials have been strategically placed in the viewing window by Protochips Inc. for verification of feature visibility and achievable contrast. These cryo-SiN specimens produced improved vitreous ice when compared with the copper TEM grid counterparts. The cryo-SiN specimens exhibited enhanced imaging contrast for independent particles, believed to lead to better reconstructions with less required data.

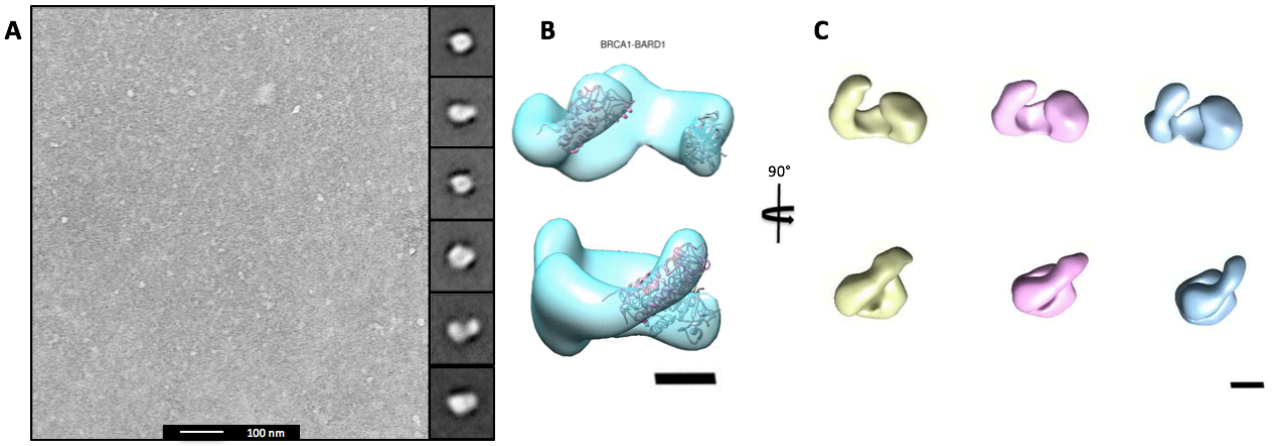

Figure 7: Investigation of wild-type BRCA1-BARD1 complexes derived from MDA-MB-361 cancer cells. A) Representative EM image and 2D class averages of BRCA1-BARD1 complexes derived from metastatic human breast cancer cells. Scale bar is 100 nm. **(B)** Atomic models of the BRCA1-BARD1 N-terminal RING, and C-terminal BRCT domains fit within EM density maps of the wild-type BRCA1 complex. Scale bar is 2 nm. **(C)** The 3D density maps of BRCA1-BARD1 complexes derived from metastatic human breast cancer cells. Scale bar is 2 nm.

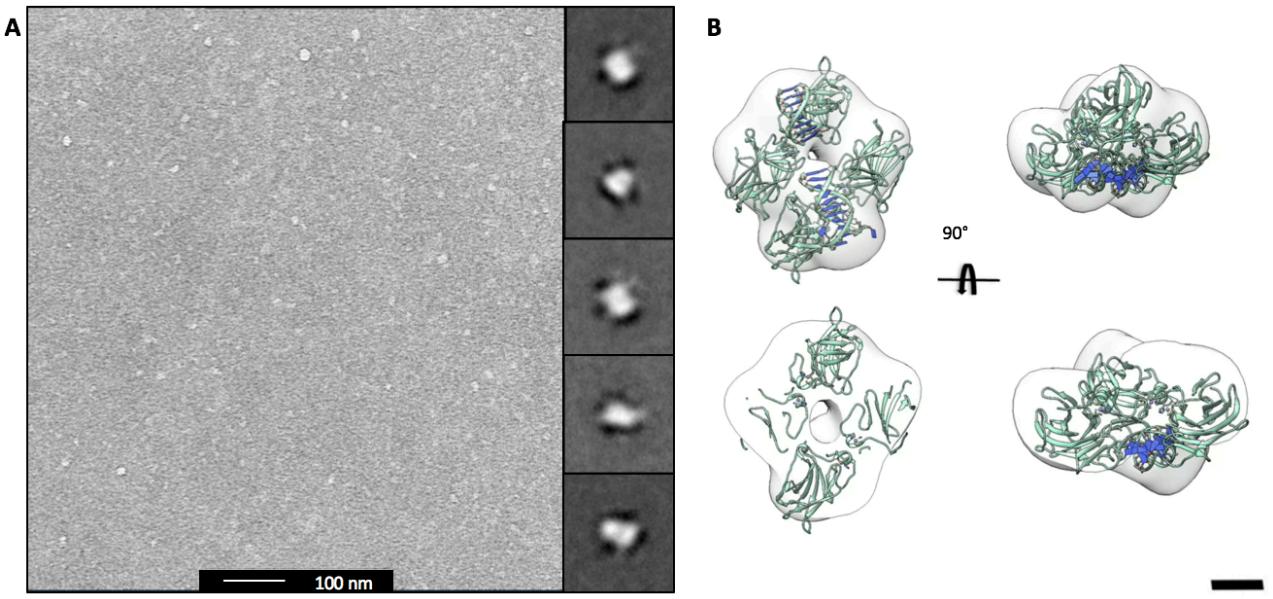

Figure 8: Investigation of wild-type p53 complexes derived from MDA-MB-361 breast cancer cells. (A) Representative EM image and 2D class averages of p53 complexes derived from metastatic human breast cancer cells. Scale bar is 20 nm. **(B)** 3D density maps of the p53 complex starting with a side view, followed by a 90º axis tilt down for a top down view show the tetrameric form of p53. Scale bar is 20 nm. The atomic model (pdb code, 2AC0), with the DNA section edited out, fit within the EM density maps of the p53 3D reconstruction (Kitayner 2006). The quality of the fit of throughout the domain is shown through a 50% cross section of the p53 model within the density map.

Additional cryo-SiN specimens remain frozen in liquid nitrogen storage for further analysis in an FEI Titan Krios equipped with a direct electron detector at Dr. Yeager's facilities at the University of Virginia School of Medicine. Dr. Yeager and Dr. Kelly shared a newly funded U24 Consortium grant that gives the Kelly lab free access to Dr. Yeager's facilities. The fully automated Titan Krios can achieve much higher quality data than the FEI Spirit BioTwin through real-time motion-correction protocols as well as high-throughput imaging procedures. This future data will also be input into the RELION software package, while implementing standard procedures to achieve higher resolution structures of BRCA1-BARD1 complexes as well as the newly discovered p53 complexes. The Kelly Lab will further enrich for p53 complexes, similar to the BRCA1 enrichment

process, using biochemical adjustments to preparative procedures.

Summary of BRCA1 Application Results:

The practicality of utilizing SiN microchips was first evaluated in the Kelly Lab's Affinity Capture technique. SiN microchips (Protochips, Inc.) were first coated with a functionalized Ni-NTA lipid monolayer trailed by binding of Protein A, then the attachment of IgG antibodies raised against BRCA1 complexes (Gilmore & Showalter et al., 2013). Due to SiN microchips having a natural hydrophobicity, they prove to be supreme substrates for the interactions between lipid tail groups, the surface of the microchip, and the air-water interface in the Ni-NTA monolayer. Negatively stained samples were additionally supplied and analyzed through TEM, and results remained consistent with previous work in the Kelly Lab leading to necessary further analysis utilizing cryo-EM procedures (Gilmore & Tanner et al., 2013). BRCA1 complexed primed amongst IgG antibodies were generously recruited toward the surface of the SiN microchips, while specimens lacking these IgG antibodies (**Figure 2C**) did not provide this tethering capability (Gilmore et al., 2015). TEM images were taken at varying magnifications (50,000x to 68,000x) to determine the aptitude of sample coverage on the SiN specimens. Based on the data received via initial negative stain studies, frozen-hydrated specimens of BRCA1 protein complexes were prepared using the cryo-SiN tunable microchip technology (**Figure 2A,B)** by plunge-freezing enriched BRCA1 samples, that also contained p53 complexes, into liquid ethane at ~-190^{o}C using the FEI VITROBOT (FEI Company) device equipped with the Gentle-Blot mechanism.

Cryo-SiN specimens were prepared under identical 100% relative humidity, 25°C conditions using 2-sided blotting for an average of 7 seconds. Upon plunge freezing in liquid ethane, the cryo-SiN specimens were quickly transferred to a 626 cryo-specimen holder (Gatan, Inc.) where they

were maintained at below -190°C in liquid nitrogen storage until further analysis in the TEM. Using the FEI Spirit BioTwin TEM operating under low-dose conditions (120 kV, 5 electrons/Å^2), images of frozen-hydrated sample were taken via an FEI 2k HS CCD camera. Visual contrast in the images were enhanced through the utilization of cryo-SiN technology (**Figure 5A**) when compared to the negative stain specimens (**Figure 6A**) under similar defocus conditions (-1.0 to -3.0 µm). Due to the enhanced visual contrast exhibited by the cryo-SiN specimens, the molecular adaptors covering the surface to form the protein tethering system were visibly distinguishable as compared to the negative stain holey carbon counterpart specimens, in which these layers were not readily discernable. Frozen-hydrated specimens not equipped with the lipid monolayer tethering system did not produce substantial protein-complex quantities, demonstrating that the tethering system does, in fact, aid in the recruitment of protein complexes away from the air-water interface. These enhanced protein-complex quantities and visual contrast results allowed for superior data collection and particle extraction and refinement processes in SPIDER and RELION for the development of 3D protein structure reconstructions.

Applications for Cryo-SiN in Reporting Related Transcriptional Assemblies:

The SiN tunable microchips were developed in the Kelly Lab, in partnership with Protochips Inc., to better capture biological assemblies from human cells as they exist in their natural state (Degen et al., 2012; Dukes et al., 2013; Winton et al., 2016). Cryo-SiN technology allows the Kelly Lab to study BRCA1-BARD1 complexes, and other binding partners, that are formed in both diseased or normal states. The tunable SiN microchips can be coated with a specialized lipid monolayer, comprised of Ni-NTA polar head groups (**Figure 4A**). The Ni-NTA polar head lipid monolayer can then be decorated with readily available His-tagged Protein A (AbCam), upon which

interchangeable IgG antibodies raised against specific protein complexes can be appended. Cellular sample is typically enriched for the protein complex of interest using techniques previously mentioned in the MDA-MB-361 BRCA1 Extraction and Sample Preparation section. This tunable interface allows for specialized cryo-EM studies as well as a supplementary advantage of isolating these delicate protein complexes away from the destructive air-water boundary layer. This technique was established through the capturing of nuclear fractionated BRCA1-bound RNA Polymerase II (RNAP II) assemblies by members in the Kelly Lab, in which negative control cryo-SiN studies deficient in the IgG antibodies were unsuccessful in sequestering the protein assemblies (Gilmore et al., 2015). In an effort to curb particle heterogeneity that can hinder resolution of structural features, flexible regions of BRCA1-BARD1 complexes were tethered to the tunable SiN microchip viewing pane.

DISCUSSION:

Prior to the introduction of new, more powerful microscopes, as well as novel sample preparation substrates, 3D reconstructions of discrete protein complexes using less than 10,000 particles would have been believed impossible. Through the development of cryo-SiN, alongside Protochips INC., as an alternative specimen substrate, the Kelly lab has been able to produce enhanced 3D models with significantly less required images and particle data. This work presents some of the first full length 3D reconstructions of metastatic BRCA1 complexes derived from human breast cancer cells through the use of cryo-SiN technology, as well as the first 3D reconstruction of p53, another highly studied protein complex. Utilizing the tunable cryo-SiN protein tethering system, we showed that BRCA1, and even p53 complexes, could be enriched for and sequestered while still preserving innate protein-protein interactions. BRCA1 complexes derived from the MDA-

MB-361 cell line exhibit the enlarged C-terminal domain due to interactions with its binding partner p53. Additionally, p53 was assessed individually through the utilization of biochemical assays and structural tools. The differences displayed between the wild-type and metastatic assemblies include decreased core flexibility and an enlarged C-terminal region among the metastatic complexes not found in the wild type assemblies. The results of this study complement previous structural studies that demonstrate the 'C-shaped' clamp-like appearance of BRCA1 complexes as well as the differences among the wild type and metastatic assemblies that had been shown in negative stain analysis on traditional EM grids.

Integral to the advancement of the life sciences, recognizing the principles that direct macromolecular developments can provide new details that have remained elusive and may previously have hindered scientific progress. Implementing conventional and cryo-EM techniques offer tools that can deliver scientists essential, structural information that can enhance current understanding of macromolecular complexes. This present work utilizes newly designed SiN microchips enclosing microwell and micropost arrays that, when used in conjunction with *in situ* TEM, allowed for the visualization of various biomedically pertinent complexes in near native states. Images of BRCA1-BARD1 and p53 complexes tethered to the SiN microchips, using functionalized Ni-NTA lipid monolayers bound to interchangeable IgG antibodies through Protein A, showed that these complexes were restricted within the microwells or micropost arrays such that any long-range diffusion was mitigated. Using the Affinity Capture tethering technique developed in the Kelly Lab, BRCA1 and p53 complexes were effectively confined within the SiN viewing array apparatus in which cryo-EM techniques revealed the face of both of these biomedically relevant complexes for further structural analysis. In addition, these studies present the first peek of near-native, frozen-hydrated BRCA1 and p53 complexes sequestered from

metastatic MDA-MB-361 breast cancer cells without the use of contrast reagents. These complexes were determined in 3D, to nearly 10 nm resolution, from 100 images and roughly 1600 particles each using the SPIDER and RELION software packages for image processing analysis.

These new studies provide further confirmation to previous work within the field, demonstrating the viability of imaging biomolecular complexes in water (Mirsaidov et al., 2012). The significance in this work utilizing cryo-SiN techniques is achieving the first 3D reconstruction of p53 as well as 3D reconstructions of metastatic MDA-MB-361 BRCA1 complexes under native conditions. In future work, high-resolution structures of both complexes in liquid using cryo-SiN technology will be feasible through the use of the high-powered Titan Krios (FEI Company) equipped with a direct electron detector. Continued studies designed to better appreciate the structural intricacy of BRCA1 assemblies and p53 complexes during various interaction stages will aid in outlining functional significance seen in these relations. Overall, the amalgamation of biochemical and structural techniques delivers the exclusive opportunity to discover native protein interactions present in both 'normal' and 'diseased' cellular progressions. Common commercially obtainable protein adaptors can supplement further SiN microchip specimen preparation toward many different disease states. Furthermore, the Affinity Capture tethering approach may one day foster unique breakthroughs on the mechanisms among native proteins that have yet to be exploited in human cancer research.

REFERENCES:

Adrian, M., Dubochet, J., Lepault, J., & Mcdowall, A. W. (1984). Cryo-electron microscopy of viruses. *Nature,308*(5954), 32-36. doi:10.1038/308032a0

Alloyeau, D., Ding, B., Ramasse, Q., Kisielowski, C., Lee, Z., & Jeon, K. (2011). Direct imaging and chemical analysis of unstained DNA origami performed with a transmission electron microscope. *Chemical Communications,47*(33), 9375. doi:10.1039/c1cc13654b

Baker, L. A., & Rubinstein, J. L. (2010). Radiation Damage in Electron Cryomicroscopy. *Methods in Enzymology Cryo-EM Part A Sample Preparation and Data Collection,*371-388. doi:10.1016/s0076-6879(10)81015-8

Beck, M., & Baumeister, W. (2016). Cryo-Electron Tomography: Can it Reveal the Molecular Sociology of Cells in Atomic Detail? *Trends in Cell Biology,26*(11), 825-837. doi:10.1016/j.tcb.2016.08.006

Brenner, S., & Horne, R. W. (1959). A negative staining method for high resolution electron microscopy of viruses. *Biochim. Biophys. Acta,34*, 103-110.

Brilot, A. F., Chen, J. Z., Cheng, A., Pan, J., Harrison, S. C., Potter, C. S., . . . Grigorieff, N. (2012). Beam-induced motion of vitrified specimen on holey carbon film. *Journal of Structural Biology,177*(3), 630-637. doi:10.1016/j.jsb.2012.02.003

Brown, L., Hovden, R., Huang, P., Wojcik, M., Muller, D. A., & Park, J. (2012). Twinning and Twisting of Tri- and Bilayer Graphene. *Nano Letters,12*(3), 1609-1615. doi:10.1021/nl204547v

Brzovic, P., Rajagopal, P., Hoyt, D., King, M., & Klevit, R. (2001). Solution structure of the BRCA1/BARD1 RING-domain heterodimer. doi:10.2210/pdb1jm7/pdb

Burton, E. F., & Oliver, W. F. (1935). X-Ray Diffraction Patterns of Ice. *Nature,135*(3413), 505-506. doi:10.1038/135505b0

Campbell, M., Cheng, A., Brilot, A., Moeller, A., Lyumkis, D., Veesler, D., . . . Grigorieff, N. (2012). Movies of Ice-Embedded Particles Enhance Resolution in Electron Cryo-Microscopy. *Structure,20*(11), 1823-1828. doi:10.1016/j.str.2012.08.026

Chen, C., Zhu, C., White, E. R., Chiu, C., Scott, M. C., Regan, B. C., . . . Miao, J. (2013). Three-dimensional imaging of dislocations in a nanoparticle at atomic resolution. *Nature,496*(7443), 74-77. doi:10.1038/nature12009

Danev, R., Buijsse, B., Khoshouei, M., Plitzko, J. M., & Baumeister, W. (2014). Volta potential phase plate for in-focus phase contrast transmission electron microscopy. *Proceedings of the National Academy of Sciences,111*(44), 15635-15640. doi:10.1073/pnas.1418377111

Dashti, A., Schwander, P., Langlois, R., Fung, R., Li, W., Hosseinizadeh, A., . . . Ourmazd, A. (2014). Trajectories of the ribosome as a Brownian nanomachine. *Proceedings of the National Academy of Sciences,111*(49), 17492-17497. doi:10.1073/pnas.1419276111

Dashti, A., Hail, D. B., Mashayekhi, G., Schwander, P., Georges, A. D., Frank, J., & Ourmazd, A. (2017). Conformational Dynamics and Energy Landscapes of Ligand Binding in RyR1. doi:10.1101/167080

Degen, K., Dukes, M., Tanner, J. R., & Kelly, D. F. (2012). The development of affinity capture devices—a nanoscale purification platform for biological in situ transmission electron microscopy. *RSC Advances,2*(6), 2408. doi:10.1039/c2ra01163h

Doerr, A. (2016). Single-particle cryo-electron microscopy. *Nature Methods,13*(1), 23-23. doi:10.1038/nmeth.3700

Dowell, L. G., & Rinfret, A. P. (1960). Low-Temperature Forms of Ice as Studied by X-Ray Diffraction. *Nature,188*(4757), 1144-1148. doi:10.1038/1881144a0

Dubochet, J., & Mcdowall, A. (1981). Vitrification Of Pure Water For Electron Microscopy. *Journal of Microscopy,124*(3), 3-4. doi:10.1111/j.1365-2818.1981.tb02483.x

Dubochet, J., Chang, J., Freeman, R., Lepault, J., & Mcdowall, A. (1982). Frozen aqueous suspensions. *Ultramicroscopy,10*(1-2), 55-61. doi:10.1016/0304-3991(82)90187-5

Dubochet, J., Lepault, J., Freeman, R., Berriman, J. A., & Homo, J. (1982). Electron microscopy of frozen water and aqueous solutions. *Journal of Microscopy,128*(3), 219-237. doi:10.1111/j.1365-2818.1982.tb04625.x

Dubochet, J., Adrian, M., Lepault, J., & Mcdowall, A. (1985). Emerging techniques: Cryo-electron microscopy of vitrified biological specimens. *Trends in Biochemical Sciences,10*(4), 143-146. doi:10.1016/0968-0004(85)90150-1

Dubochet, J. (2011). Cryo-EM-the first thirty years. *Journal of Microscopy,245*(3), 221-224. doi:10.1111/j.1365-2818.2011.03569.x

Dubochet, J., Adrian, M., Chang, J., Lepault, J., & Mcdowall, A. W. (1987). Cryoelectron Microscopy of Vitrified Specimens. *Cryotechniques in Biological Electron Microscopy,*114-131. doi:10.1007/978-3-642-72815-0_5

Dubochet, J., Adrian, M., Chang, J., Lepault, J., & Mcdowall, A. W. (1987). Cryoelectron Microscopy of Vitrified Specimens. *Cryotechniques in Biological Electron Microscopy,*114-131. doi:10.1007/978-3-642-72815-0_5

Dukes, M. J., Thomas, R., Damiano, J., Klein, K. L., Balasubramaniam, S., Kayandan, S., . . . Kelly, D. F. (2013). Improved Microchip Design and Application for In Situ Transmission Electron Microscopy of Macromolecules. *Microscopy and Microanalysis,20*(02), 338-345. doi:10.1017/s1431927613013858

Erickson, H. P., & Klug, A. (1971). Measurement and Compensation of Defocusing and Aberrations by Fourier Processing of Electron Micrographs. *Philosophical Transactions of the Royal Society B: Biological Sciences,261*(837), 105-118. doi:10.1098/rstb.1971.0040

Faruqi, A., Henderson, R., Pryddetch, M., Allport, P., & Evans, A. (2006). Erratum to: "Direct single electron detection with a CMOS detector for electron microscopy". *Nuclear Instruments and Methods in Physics Research Section A: Accelerators, Spectrometers, Detectors and Associated Equipment,566*(2), 770. doi:10.1016/j.nima.2006.07.013

Faruqi, A., Cattermole, D. M., & Raeburn, C. (2007). Direct Electron Detectors for Electron Microscopy. *Advances in Imaging and Electron Physics,*55-93. doi:10.1016/s1076-5670(06)45002-3

Fernández-Morán, H. (2006). Low-Temperature Preparation Techniques For Electron Microscopy Of Biological Specimens Based On Rapid Freezing With Liquid Helium Ii*. *Annals of the New York Academy of Sciences,85*(2), 689-713. doi:10.1111/j.1749-6632.1960.tb49990.x

Fischer, N., Konevega, A. L., Wintermeyer, W., Rodnina, M. V., & Stark, H. (2010). Ribosome dynamics and tRNA movement by time-resolved electron cryomicroscopy. *Nature,466*(7304), 329-333. doi:10.1038/nature09206

Frank, J., & Al-Ali, L. (1975). Signal-to-noise ratio of electron micrographs obtained by cross correlation. *Nature,256*(5516), 376-379. doi:10.1038/256376a0

Frank, J., Goldfarb, W., Eisenberg, D., & Baker, T. (1979). Addendum to "Reconstruction of glutamine synthetase using computer averaging". *Ultramicroscopy,4*(2), 247. doi:10.1016/s0304-3991(79)90319-x

Frank, J., & Heel, M. V. (1982). Correspondence analysis of aligned images of biological particles. *Journal of Molecular Biology,161*(1), 134-137. doi:10.1016/0022-2836(82)90282-0

Frank, J. (1975). Averaging of low exposure electron micrographs of non-periodic objects. *Ultramicroscopy,1*(2), 159-162. doi:10.1016/s0304-3991(75)80020-9

Frank, J., Shimkin, B., & Dowse, H. (1981). Spider—A modular software system for electron image processing. *Ultramicroscopy,6*(4), 343-357. doi:10.1016/s0304-3991(81)80236-7

Frank, J. (1996). Three-Dimensional Reconstruction. *Three-Dimensional Electron Microscopy of Macromolecular Assemblies,*182-246. doi:10.1016/b978-012265040-6/50005-9

Frank, J., Radermacher, M., Penczek, P., Zhu, J., Li, Y., Ladjadj, M., & Leith, A. (1996). SPIDER and WEB: Processing and Visualization of Images in 3D Electron Microscopy and Related Fields. *Journal of Structural Biology,116*(1), 190-199. doi:10.1006/jsbi.1996.0030

Gaietta, G. (2002). Multicolor and Electron Microscopic Imaging of Connexin Trafficking. *Science,296*(5567), 503-507. doi:10.1126/science.1068793

Gilmore, B., Tanner, J., Mckell, A., Boudreaux, C., Dukes, M., Mcdonald, S., & Kelly, D. (2013). Molecular Surveillance of Viral Processes Using Silicon Nitride Membranes. *Micromachines,4*(4), 90-102. doi:10.3390/mi4010090

Gilmore, B. L., Showalter, S. P., Dukes, M. J., Tanner, J. R., Demmert, A. C., Mcdonald, S. M., & Kelly, D. F. (2013). Visualizing viral assemblies in a nanoscale biosphere. *Lab Chip,13*(2), 216-219. doi:10.1039/c2lc41008g

Gilmore, B. L., Winton, C. E., Demmert, A. C., Tanner, J. R., Bowman, S., Karageorge, V., . . . Kelly, D. F. (2015). A Molecular Toolkit to Visualize Native Protein Assemblies in the Context of Human Disease. *Scientific Reports,5*(1). doi:10.1038/srep14440

Glaeser, R. M. (1999). Review: Electron Crystallography: Present Excitement, a Nod to the Past, Anticipating the Future. *Journal of Structural Biology,128*(1), 3-14. doi:10.1006/jsbi.1999.4172

Haas, D. J. (1968). X-ray studies on lysozyme crystals at –50°C. *Acta Crystallographica Section B Structural Crystallography and Crystal Chemistry,24*(4), 604-604. doi:10.1107/s056774086800292x

Haas, D. J., & Rossmann, M. G. (1970). Crystallographic Studies on Lactate Dehydrogenase at −75°C. *Acta Crystallogr,B 26*, 998-1004. doi:10.1142/9789814513357_0011

Hall, C. E., Jakus, M. A., & Schmitt, F. O. (1945). The Structure of Certain Muscle Fibrils as Revealed by the Use of Electron Stains. *Journal of Applied Physics,16*(8), 459-465. doi:10.1063/1.1707615

Heel, M. V., & Frank, J. (1981). Use of multivariates statistics in analysing the images of biological macromolecules. *Ultramicroscopy,6*(1), 187-194. doi:10.1016/s0304-3991(81)80197-0

Henderson, R., Baldwin, J., Ceska, T., Zemlin, F., Beckmann, E., & Downing, K. (1991). Model For The Structure Of Bacteriorhodopsin Based On High-Resolution Electron Cryo-Microscopy. *J. Mol. Biol.,213*, 899-929. doi:10.2210/pdb1brd/pdb

Henderson, R. (1995). The potential and limitations of neutrons, electrons and X-rays for atomic resolution microscopy of unstained biological molecules. *Quarterly Reviews of Biophysics,28*(02), 171. doi:10.1017/s003358350000305x

Hite, R. K., & MacKinnon, R. (2017). Structural titration of Slo2.2, a Na -dependent K channel. *Cell,168*, 390-399.

Huxley, H. E. (1961). Preferential Staining Of Nucleic Acid-Containing Structures For Electron Microscopy. *The Journal of Cell Biology,11*(2), 273-296. doi:10.1083/jcb.11.2.273

Jenniskens, P., & Blake, D. (1994). Structural transitions in amorphous water ice and astrophysical implications. *Science,265*(5173), 753-756. doi:10.1126/science.11539186

Kam, J., Demmert, A. C., Tanner, J. R., Mcdonald, S. M., & Kelly, D. F. (2014). Structural dynamics of viral nanomachines. *Technology,02*(01), 44-48. doi:10.1142/s2339547814500034

Kelly, D. F., Abeyrathne, P. D., Dukovski, D., & Walz, T. (2008). The Affinity Grid: A Pre-fabricated EM Grid for Monolayer Purification. *Journal of Molecular Biology,382*(2), 423-433. doi:10.1016/j.jmb.2008.07.023

Khoshouei, M., Radjainia, M., Bunker, R., Baumeister, W., & Danev, R. (2017). CryoEM structure of haemoglobin at 3.2 A determined with the Volta phase plate. doi:10.2210/pdb5ni1/pdb

Kitayner, M., Rozenberg, H., Kessler, N., Rabinovich, D., & Shakked, Z. (2006). Structural Basis of DNA Recognition by p53 Tetramers (complex II). doi:10.2210/pdb2ata/pdb

Klug, A. (1965). Structure of viruses of the papilloma-polyoma type. *Journal of Molecular Biology,11*(2). doi:10.1016/s0022-2836(65)80067-5

Klug, A., & Rosier, D. J. (1966). Optical Filtering of Electron Micrographs: Reconstruction of One-Sided Images. *Nature,212*(5057), 29-32. doi:10.1038/212029a0

Kuhlbrandt, W. (2014). The Resolution Revolution. *Science,343*(6178), 1443-1444. doi:10.1126/science.1251652

Lawton, J., Estes, M., & Prasad, B. V. (1997). Three-dimensional visualization of mRNA release from actively transcribing rotavirus particles. *Nature Structural Biology,4*(2), 118-121. doi:10.1038/nsb0297-118

Lepault, J., Booy, F. P., & Dubochet, J. (1983). Electron microscopy of frozen biological suspensions. *Journal of Microscopy,129*(1), 89-102. doi:10.1111/j.1365-2818.1983.tb04163.x

Li, X., Mooney, P., Zheng, S., Booth, C. R., Braunfeld, M. B., Gubbens, S., . . . Cheng, Y. (2013). Electron counting and beam-induced motion correction enable near-atomic-resolution single-particle cryo-EM. *Nature Methods,10*(6), 584-590. doi:10.1038/nmeth.2472

Liang, Y., Dearnaley, W. J., Varano, A. C., Winton, C. E., Gilmore, B. L., Alden, N. A., . . . Kelly, D. F. (2017). Structural analysis of BRCA1 reveals modification hotspot. *Science Advances,3*(9). doi:10.1126/sciadv.1701386

Liao, M., Cao, E., Julius, D., & Cheng, Y. (2013). Structure of TRPV1 ion channel determined by single particle electron cryo-microscopy. *Nature,504*, 107-112. doi:10.2210/pdb3j5p/pdb

Marton, L. (1934). Electron Microscopy of Biological Objects. *Nature,133*(3372), 911-911. doi:10.1038/133911b0

Mcmullan, G., Clark, A., Turchetta, R., & Faruqi, A. (2009). Enhanced imaging in low dose electron microscopy using electron counting. *Ultramicroscopy,109*(12), 1411-1416. doi:10.1016/j.ultramic.2009.07.004

Mcmullan, G., Faruqi, A., & Henderson, R. (2016). Direct Electron Detectors. *Methods in Enzymology The Resolution Revolution: Recent Advances In cryoEM,*1-17. doi:10.1016/bs.mie.2016.05.056

Milazzo, A., Leblanc, P., Duttweiler, F., Jin, L., Bouwer, J. C., Peltier, S., . . . Xuong, N. (2005). Active pixel sensor array as a detector for electron microscopy. *Ultramicroscopy,104*(2), 152-159. doi:10.1016/j.ultramic.2005.03.006

Mirsaidov, U., Zheng, H., Casana, Y., & Matsudaira, P. (2012). Imaging Protein Structure in Water at 2.7 nm Resolution by Transmission Electron Microscopy. *Biophysical Journal,102*(4). doi:10.1016/j.bpj.2012.01.009

Oikonomou, C. M., & Jensen, G. J. (2017). Cellular Electron Cryotomography: Toward Structural Biology In Situ. *Annual Review of Biochemistry,86*(1), 873-896. doi:10.1146/annurev-biochem-061516-044741

Peckys, D. B., Dukes, M. J., & Jonge, N. D. (2013). Correlative Fluorescence and Electron Microscopy of Quantum Dot Labeled Proteins on Whole Cells in Liquid. *Methods in Molecular Biology Electron Microscopy,*527-540. doi:10.1007/978-1-62703-776-1_23

Pettersen, E. F., Goddard, T. D., Huang, C. C., Couch, G. S., Greenblatt, D. M., Meng, E. C., & Ferrin, T. E. (2004). UCSF Chimera?A visualization system for exploratory research and analysis. *Journal of Computational Chemistry,25*(13), 1605-1612. doi:10.1002/jcc.20084

Radermacher, M. (1980). Dreidimensionale Rekonstruktion bei kegelförmiger Kippung im Elektronenmikroskop. *Thesis, Technical University, Munich*.

Radermacher, M., Wagenknecht, T., Verschoor, A., & Frank, J. (1986). A New 3-D Reconstruction Scheme Applied To The 50S Ribosomal Subunit Of E. Coli. *Journal of Microscopy,141*(1). doi:10.1111/j.1365-2818.1986.tb02693.x

Radermacher, M., Wagenknecht, T., Verschoor, A., & Frank, J. (1987). Three-dimensional reconstruction from a single-exposure, random conical tilt series applied to the 50S ribosomal subunit of Escherichia coli. *Journal of Microscopy,146*(2), 113-136. doi:10.1111/j.1365-2818.1987.tb01333.x

Rhinow, D., & Kühlbrandt, W. (2008). Electron cryo-microscopy of biological specimens on conductive titanium–silicon metal glass films. *Ultramicroscopy,108*(7), 698-705. doi:10.1016/j.ultramic.2007.11.005

Ring, E. A., Peckys, D. B., Dukes, M. J., Baudoin, J. P., & Jonge, N. D. (2011). Silicon nitride windows for electron microscopy of whole cells. *Journal of Microscopy,243*(3), 273-283. doi:10.1111/j.1365-2818.2011.03501.x

Ring, E. A., & Jonge, N. D. (2010). Microfluidic System for Transmission Electron Microscopy. *Microscopy and Microanalysis,16*(05), 622-629. doi:10.1017/s1431927610093669

Ripstein, Z., & Rubinstein, J. (2016). Processing of Cryo-EM Movie Data. *Methods in Enzymology The Resolution Revolution: Recent Advances In cryoEM,*103-124. doi:10.1016/bs.mie.2016.04.009

DeRosier, D. J., & Klug, A. (1968). Reconstruction of Three Dimensional Structures from Electron Micrographs. *Nature,217*(5124), 130-134. doi:10.1038/217130a0

Rubinstein, J. L., & Brubaker, M. A. (2015). Alignment of cryo-EM movies of individual particles by optimization of image translations. *Journal of Structural Biology,192*(2), 188-195. doi:10.1016/j.jsb.2015.08.007

Rubinstein, J. L. (2017). Cryo-EM Captures the Dynamics of Ion Channel Opening. *Cell,168*(3), 341-343. doi:10.1016/j.cell.2017.01.011

Saxton, W., & Frank, J. (1976). Motif detection in quantum noise-limited electron micrographs by cross-correlation. *Ultramicroscopy,2*, 219-227. doi:10.1016/s0304-3991(76)91385-1

Scheres, S. H., Gao, H., Valle, M., Herman, G. T., Eggermont, P. P., Frank, J., & Carazo, J. (2006). Disentangling conformational states of macromolecules in 3D-EM through likelihood optimization. *Nature Methods,4*(1), 27-29. doi:10.1038/nmeth992

Scheres, S. H. (2012). A Bayesian view on cryo-EM structure determination. *2012 9th IEEE International Symposium on Biomedical Imaging (ISBI)*. doi:10.1109/isbi.2012.6235807

Schmidt, P. (2006). Basile J. Luyet and the Beginnings of Transfusion Cryobiology. *Transfusion Medicine Reviews,20*(3), 242-246. doi:10.1016/j.tmrv.2006.03.004

Scott, M. C., Chen, C., Mecklenburg, M., Zhu, C., Xu, R., Ercius, P., . . . Miao, J. (2012). Electron tomography at 2.4-ångström resolution. *Nature,483*(7390), 444-447. doi:10.1038/nature10934

Sigworth, F. (1998). A Maximum-Likelihood Approach to Single-Particle Image Refinement. *Journal of Structural Biology,122*(3), 328-339. doi:10.1006/jsbi.1998.4014

Suloway, C., Pulokas, J., Fellmann, D., Cheng, A., Guerra, F., Quispe, J., . . . Carragher, B. (2005). Automated molecular microscopy: The new Leginon system. *Journal of Structural Biology,151*(1), 41-60. doi:10.1016/j.jsb.2005.03.010

Taylor, K. A., & Glaeser, R. M. (1974). Electron Diffraction of Frozen, Hydrated Protein Crystals. *Science,186*(4168), 1036-1037. doi:10.1126/science.186.4168.1036

Taylor, K. A., & Glaeser, R. M. (1976). Electron microscopy of frozen hydrated biological specimens. *Journal of Ultrastructure Research,55*(3), 448-456. doi:10.1016/s0022-5320(76)80099-8

Varano, A. C., Harafuji, N., Dearnaley, W., Guay-Woodford, L., & Kelly, D. F. (2017). Preparation of Disease-Related Protein Assemblies for Single Particle Electron Microscopy. *Methods in Molecular Biology Proteomics for Drug Discovery,*185-196. doi:10.1007/978-1-4939-7201-2_12

Vlassak, J., & Nix, W. (1992). A new bulge test technique for the determination of Youngs modulus and Poissons ratio of thin films. *Journal of Materials Research,7*(12), 3242-3249. doi:10.1557/jmr.1992.3242

Williams, R., Green, R., & Glover, J. (2001). Crystal structure of the BRCT repeat region from the breast cancer associated protein, BRCA1. doi:10.2210/pdb1jnx/pdb

Winton, C. E., Gilmore, B. L., Demmert, A. C., Karageorge, V., Sheng, Z., & Kelly, D. F. (2016). A microchip platform for structural oncology applications. *Npj Breast Cancer,2*(1). doi:10.1038/npjbcancer.2016.16

Xuong, N., Milazzo, A., Leblanc, P., Duttweiler, F., Bouwer, J., Peltier, S., . . . Kleinfelder, S. (2004). First use of a high-sensitivity active pixel sensor array as a detector for electron microscopy. *Sensors and Camera Systems for Scientific, Industrial, and Digital Photography Applications V*. doi:10.1117/12.526021

Yoshioka, C., Carragher, B., & Potter, C. S. (2010). Cryomesh™: A New Substrate for Cryo-Electron Microscopy. *Microscopy and Microanalysis,16*(01), 43-53. doi:10.1017/s1431927609991310

Yuk, J. M., Park, J., Ercius, P., Kim, K., Hellebusch, D. J., Crommie, M. F., . . . Alivisatos, A. P. (2012). High-Resolution EM of Colloidal Nanocrystal Growth Using Graphene Liquid Cells. *Science,336*(6077), 61-64. doi:10.1126/science.1217654

Zhang, X., Settembre, E., Xu, C., Dormitzer, P. R., Bellamy, R., Harrison, S. C., & Grigorieff, N. (2008). Near-atomic resolution using electron cryomicroscopy and single-particle reconstruction. *Proceedings of the National Academy of Sciences,105*(6), 1867-1872. doi:10.1073/pnas.0711623105

Zhao, J., Benlekbir, S., & Rubinstein, J. L. (2015). Electron cryomicroscopy observation of rotational states in a eukaryotic V-ATPase. *Nature,521*(7551), 241-245. doi:10.1038/nature14365

APPENDIX A:

*Note: The following protocols have been filed with the Virginia Tech Intellectual Property (VTIP) corporation on behalf of Dr. Kelly and the Kelly lab, all rights reserved.

Protocol Objective:

The objective is to determine the affinity of BRCA1 binding capability as well as the affinity of BRCA1-RNA Polymerase II in multiple testing scenarios such as application of oxidative stress as well as testing with natural and mutant forms of BRCA1, ubiquitinated and ubiquitin cleaved BRCA1, and how these various forms interact with its main binding partners such as BARD1, and p53, etc.

Needed Materials and Necessary Buffer Recipes

1x PBS Wash Buffer: Dissolve the following in 800 mL distilled H_2O

- 8g of NaCl
- 0.2g of KCl

- 1.44g of Na_2HPO_4
- 0.24g of KH_2PO_4

Adjust to pH of 7.4 with HCl, and then adjust the volume to 1L with additional distilled H_2O as needed. Sterilize by autoclaving.

10x TBS Wash Buffer: Dissolve the following in 900mL of distilled H_2O

- 24g of Tris-HCl (Formula weight: 157.6g)
- 5.6g of Tris Base (Formula weight: 121.1g)
- 88g NaCl (formula weight: 58.4g)

Adjust the pH of the solution to 7.6 at room temperature *(If too basic use concentrated HCl / If too acidic use concentrated NaOH)* and then adjust the volume to 1L with additional distilled H_2O.

CAUTION: OSHA considers HCl and NaOH to be hazardous materials. Exercise caution when working with these materials, and in order to avoid any risks involved in using these materials please take all possible precautionary measures for protection such as wearing personal protective equipment, as well as following your local, regional, national and international legislation. Please refer to the MSDS of both HCl and NaOH for more information regarding the associated health and safety guidelines.

TBS-T Wash Buffer: Dissolve the following in 900mL distilled H_2O

- 100mL 10x TBS
- 500uL Tween 20

1% NFDM:

- 2g of NFDM
- 200mL of TBS-T

Nuclear Extract containing BRCA1

- Vortex tube on high for 15 seconds
- Incubate on ice for 10 minutes
- Add cold CER II to the tube
- Vortex on high again for 5 seconds
- Incubate on ice for 1 minute
- Vortex on high again for 5 seconds
- Centrifuge the tube for 5 minutes at max speed at 4 degrees Celsius
- Transfer the supernatant (Cytoplasmic Extract, CE) to a clean, pre chilled tube and place on ice
- Suspend the insoluble pellet in cold NER
- Vortex on high again for 15 seconds every 10 minutes for 40 minutes; 10 20 30 40
- Centrifuge at 16,000g for 10 minutes at 4 degrees Celsius
- Transfer supernatant (Nuclear Extract, NE) to clean, prefilled tube and place on ice
- Store at -80 degrees Celsius until ready to use

Necessary volume of each of the following: E2+E3 mixture at concentrations of 1:1, 1:2, 1:4, 1:8, 1:16, 1:32, 1:64, 1:256, 1:512, 1:1024 [or as necessary] in buffer solution.

Prepare 1 mg/ml Lipid Solutions of DLPC and Ni-NTA using only proper GC Syringes and Glass tubes

- 1 mg DLPC in 1 ml of $CHCl_3$
- 1 mg Ni-NTA in 1 ml of $CHCl_3$

CAUTION: OSHA considers $CHCl_3$ to be hazardous. Exercise caution when working with this material, and in order to avoid any risks involved in using this material please take all possible precautionary measures for protection such as wearing personal protective equipment, as well as following your local, regional, national and international legislation. Please refer to the MSDS of $CHCl_3$ for more information regarding the associated health and safety guidelines. Use under fume hood for proper safety.

Prepare 25% Ni-NTA enriched lipids using proper GC Syringes and Glass tubes
Mix $CHCl_3$, DLPC, and Ni-NTA to final percent volume concentrations of 25%, 50%, and 25% respectively. Ex…

- 10ul $CHCl_3$
- 20ul 1 mg/ml DLPC
- 10ul 1 mg/ml Ni-NTA

BRCA1 (c-20 or k-48) with a dilution factor of 1:1000

Goat anti-rabbit conjugated with HRP for (c-20 or k-48) as primary antibody in dilution of 1:50,000

TMB ELISA Reagent
- Peroxidase Substrate
- Peroxide Solution

CAUTION: Peroxidase Substrate is considered hazardous by the OSHA Hazard Communication Standard (29 CFR 1910.1200). Exercise caution when working with this material, and in order to avoid any risks involved in using this material please take all possible precautionary measures for protection such as wearing personal protective equipment, as well as following your local, regional, national and international legislation. Please refer to the MSDS of Peroxidase Substrate (TMB) for more information regarding the associated health and safety guidelines.

P20, P200, P1000 pipets and GC syringes, and glass tubes

96-Well Polypropylene ELISA Plate

Micro-Titer Plate Reader

Coating Plate with Capture Ni-NTA Enriched Lipids

1. Prepare capture 25% Ni-NTA enriched lipids in either $CHCl_3$ or DMSO for the polypropylene and polystyrene plates respectively. *($CHCl_3$ and polystyrene have notable chemical compatibility issues as seen in chemical compatibility charts)*
2. Coat wells of a 96 well plate with 5uL of capture 25% Ni-NTA enriched lipids. *(Perform tests in duplicate at minimum)*
3. Wrap plate in plastic to incubate overnight at room temperature.
4. Rinse plate with 25 ul wash buffer TBS-T three times.
5. Block residual binding capacity of plate filling each well with 25 ul of blocking buffer NFDM and incubate for 15 minutes at room temperature.
6. Rinse three times with 25 ul wash buffer TBS-T and tap residual rinse onto a paper towel.

Prepare Antigen: BRCA1

7. Prepare a standard antigen-dilution series by successive serial dilutions of the test sample in blocking buffer [0.1 – 1000 ng/ml]. *(Refer to support protocol)*
8. Prepare dilutions of test sample solutions from nuclear extraction in blocking buffer.
9. Add [5uL] of antigen test solutions and the serial dilutions of standard antigen dilutions to the antibody coated wells, then wrap in plastic and incubate for a minimum of 2 hours at room temperature or overnight at 4°C. *(Perform tests in duplicate at minimum) – Could heat at 37℃ for faster incubation.*
10. Rinse coated plate with 25 ul TBS-t three times.

11. Block residual binding capacity of plate filling each well with 25 ul of blocking buffer NFDM and incubating for 30 minutes at room temperature.
12. Rinse three times with 25 ul TBS-T and tap residual water onto a paper towel.

Add Primary Antibody and Secondary Antibody-Enzyme Conjugate

13. Add (5 ul) of [specific primary antibody – BRCA1 sc-642 (c-20) or k-48] of concentration 1:1000 then wrap in plastic and incubate for a minimum of 2 hours at room temperature. *(Perform tests in duplicate at minimum) – Could heat at 37℃ for faster incubation.*
14. Rinse coated plate with 25 ul wash buffer three TBS-T times.
15. Block residual binding with 25 ul blocking buffer NFDM, then vortex and incubate for 15 minutes.
16. Rinse coated plate with 25 ul wash buffer TBS-T three times.
17. Add (5 ul) of [specific secondary antibody/enzyme conjugate dilution – goat anti-rabbit conjugated with HRP *(goat anti-mouse if capture and primary antibodies are flipped)]* then wrap in plastic and incubate for a minimum of 2 hours at room temperature.
18. Rinse coated plate with 25 ul wash buffer TBS-T three times.
19. Block residual binding with 25 ul blocking buffer NFDM, then (vortex) and incubate for 15 minutes.
20. Rinse coated plate with 25 ul wash buffer TBS-T three times.
21. Add (25 ul) of [TMB solution or HRP-hydrogen peroxide substrate] to each well and incubate for 15-30 minutes at room temperature.
22. *Read plate on Microtiter plate reader.*
23. *Prepare Standard Curve, Interpolate.*

Although better results were ultimately achieved through the use of the first protocol the following, secondary protocol, is as follows:

Needed Materials and Necessary Buffer Recipes

1x PBS Wash Buffer: Dissolve the following in 800 mL distilled H_2O

- 8g of NaCl
- 0.2g of KCl

- 1.44g of Na_2HPO_4
- 0.24g of KH_2PO_4

Adjust to pH of 7.4 with HCl, and then adjust the volume to 1L with additional distilled H_2O as needed. Sterilize by autoclaving.

10x TBS Wash Buffer: Dissolve the following in 900mL of distilled H_2O

- 24g of Tris-HCl (Formula weight: 157.6g)
- 5.6g of Tris Base (Formula weight: 121.1g)
- 88g NaCl (formula weight: 58.4g)

Adjust the pH of the solution to 7.6 at room temperature *(If too basic use concentrated HCl / If too acidic use concentrated NaOH)* and then adjust the volume to 1L with additional distilled H_2O.

CAUTION: OSHA considers HCl and NaOH to be hazardous materials. Exercise caution when working with these materials, and in order to avoid any risks involved in using this material please take all possible precautionary measures for protection such as wearing personal protective equipment, as well as following your local, regional, national and international legislation. Please refer to the MSDS of both HCl and NaOH for more information regarding the associated health and safety guidelines.

TBS-T Wash Buffer: Dissolve the following in 900mL distilled H_2O

- 100mL 10x TBS
- 500uL Tween 20

1% NFDM:

- 2g of NFDM
- 200mL of TBS-T

Nuclear Extract containing BRCA1

- Vortex tube on high for 15 seconds
- Incubate on ice for 10 minutes
- Add cold CER II to the tube
- Vortex on high again for 5 seconds
- Incubate on ice for 1 minute
- Vortex on high again for 5 seconds
- Centrifuge the tube for 5 minutes at max speed at 4 degrees Celsius
- Transfer the supernatant (Cytoplasmic Extract, CE) to a clean, pre chilled tube and place on ice
- Suspend the insoluble pellet in cold NER
- Vortex on high again for 15 seconds every 10 minutes for 40 minutes; 10 20 30 40
- Centrifuge at 16,000g for 10 minutes at 4 degrees Celsius
- Transfer supernatant (Nuclear Extract, NE) to clean, prefilled tube and place on ice
- Store at -80 degrees Celsius until ready to use

Necessary volume of each of the following: E2+E3 mixture at concentrations of 1:1, 1:2, 1:4, 1:8, 1:16, 1:32, 1:64, 1:256, 1:512, 1:1024 [or as necessary] in buffer solution.

Prepare capture antibody by diluting BRCA1 c-20 and Ab-1 in PBSN to final concentrations of 0.2, 0.6 and 1.0 ug/ml

BRCA1 sc-642 and c-20 with a dilution factor of 1:1000

Goat anti-rabbit conjugated with HRP for c-20 as primary antibody and goat anti-mouse if the primary antibody is Ab-1 in dilutions of 1:50,000 and 1:20,000 respectively

TMB ELISA Reagent

- Peroxidase Substrate
- Peroxide Solution

CAUTION: This material is considered hazardous by the OSHA Hazard Communication Standard (29 CFR 1910.1200). Exercise caution when working with this material, and in order to avoid any risks involved in using this material please take all possible precautionary measures for protection such as wearing personal protective equipment, as well as following your local, regional, national and international legislation. Please refer to the MSDS of Peroxidase Substrate (TMB) for more information regarding the associated health and safety guidelines.

P20, P200, P1000 pipets
96-Well Polystyrene ELISA Plate
Micro-Titer Plate Reader

Coating Plate with Capture Antibody

24. Prepare capture antibody by diluting [specific antibody] in 1x PBS to a final concentration of 0.1 to 10 ug/ml. Concentration of _____ to be used. Monoclonal or Polyclonal: [BRCA1 OP92 monoclonal antibody (C-20)]. *(Use criss-cross serial dilution analysis to determine concentration of capture antibody to use) *Note: C20-k48-GantiRb HRP leads to poor experimental results as does Ab1-k48-Goat anti Rabbit HRP*
25. Coat wells of a 96 well plate with 50uL of capture antibody solution. *(Perform tests in duplicate at minimum)*
26. Wrap plate in plastic to incubate overnight at room temperature.
27. Rinse plate with 100ul wash buffer TBS-T three times.
28. Block residual binding capacity of plate filling each well with 100uL of blocking buffer NFDM and incubate for 15 minutes at room temperature.
29. Rinse three times with 100ul wash buffer TBS-T and tap residual rinse onto a paper towel.

Prepare Antigen: BRCA1

30. Prepare a standard antigen-dilution series by successive serial dilutions of the test sample in blocking buffer [0.1 – 1000 ng/ml]. *(Refer to support protocol)*
31. Prepare dilutions of test sample solutions from nuclear extraction in blocking buffer.
32. Add [50uL] of antigen test solutions and the serial dilutions of standard antigen dilutions to the antibody coated wells, then wrap in plastic and incubate for a minimum of 2 hours at room temperature or overnight at 4°C. *(Perform tests in duplicate at minimum) – Could heat at 37℃ for faster incubation.*
33. Rinse coated plate with TBS-t three times.
34. Block residual binding capacity of plate filling each well with 100 ul of blocking buffer NFDM and incubating for 15 minutes at room temperature.
35. Rinse three times with TBS-T and tap residual water onto a paper towel.
    Add Primary Antibody and Secondary Antibody-Enzyme Conjugate

36. Add (50 ul) of [specific primary antibody – BRCA1 sc-642 (c-20)] of concentration [~0.2 ug/ml], then wrap in plastic and incubate for a minimum of 2 hours at room temperature. *(Perform tests in duplicate at minimum) – Could heat at 37℃ for faster incubation.*

37. Rinse coated plate with 100ul wash buffer three TBS-T times.
38. Block residual binding with 100ul blocking buffer NFDM, then vortex and incubate for 15 minutes.
39. Rinse coated plate with 100ul wash buffer TBS-T three times.
40. Add (50 ul) of [specific secondary antibody/enzyme conjugate dilution – goat anti-rabbit conjugated with HRP *(goat anti-mouse if capture and primary antibodies are flipped)]* then wrap in plastic and incubate for a minimum of 2 hours at room temperature.
41. Rinse coated plate with 100ul wash buffer TBS-T three times.
42. Block residual binding with 100ul blocking buffer NFDM, then (vortex) and incubate for 15 minutes.
43. Rinse coated plate with 100ul wash buffer TBS-T three times.
44. Add (100 ul) of [TMB solution or HRP-hydrogen peroxide substrate] to each well and incubate for 15-30 minutes at room temperature.
45. *Read plate on Microtiter plate reader.*
46. *Prepare Standard Curve, Interpolate.*

Table A1: Possible plate setup for sample optimization procedures.

	1	2	3	4	5	6	7	8	9	10	11	12
A	SD: 2	SD: 1.5	SD: 1	SD: 0.75	SD: 0.5	SD: 0.25	SD: 0.125	SD: 0.025	#			
B	SD: 2	SD: 1.5	SD: 1	SD: 0.75	SD: 0.5	SD: 0.25	SD: 0.125	SD: 0.025	#			
C	nat 1:10	nat 1:20	mut 1:10	mut 1:20	pol 1:10	pol 1:20	nat 1:10	nat 1:20	mut 1:10	mut 1:20	pol 1:10	pol 1:20
D	nat 1:10	nat 1:20	mut 1:10	mut 1:20	pol 1:10	pol 1:20	nat 1:10	nat 1:20	mut 1:10	mut 1:20	pol 1:10	pol 1:20
E	OS nat 1:10	OS nat 1:20	OS mut 1:10	OS mut 1:20	OS pol 1:10	OS pol 1:20	OS nat 1:10	OS nat 1:20	OS mut 1:10	OS mut 1:20	OS pol 1:10	OS pol 1:20
F	OS nat 1:10	OS nat 1:20	OS mut 1:10	OS mut 1:20	OS pol 1:10	OS pol 1:20	OS nat 1:10	OS nat 1:20	OS mut 1:10	OS mut 1:20	OS pol 1:10	OS pol 1:20
G												
H												

*Note: Concentration dilution ratios come from pre-established sample concentrations and are subject to change give the concentration one wants to achieve.

SD	Serial Dilution of Nuclear Extract (ug/ml)
nat	Wild-Type BRCA1 Antigen (1:10 and 1:20 are dilution ratios)
mut	Mutant BRCA1 Antigen (… see above)
pol	BRCA1 – Polymerase interaction (… see above)
OS	Oxidative Stress application
*Highlight	Possible switching of Capture and Primary Antibody type
#	HEPES Buffer

Table A2: Possible plate setup for optimization of antibody concentrations.

*A-C in (ug/ml)	1	2	3	4	5	6	7	8	9	10	11	12
A	3 / 3 / 1	3 / 6 / 1	3 / 9 / 1	6 / 3 / 1	6 / 6 / 1	6 / 9 / 1	9 / 3 / 1	9 / 6 / 1	9 / 9 / 1			
B	3 / 3 / 2.5	3 / 6 / 2.5	3 / 9 / 2.5	6 / 3 / 2.5	6 / 6 / 2.5	6 / 9 / 2.5	9 / 3 / 2.5	9 / 6 / 2.5	9 / 9 / 2.5			
C	3 / 3 / 4	3 / 6 / 4	3 / 9 / 4	6 / 3 / 4	6 / 6 / 4	6 / 9 / 4	9 / 3 / 4	9 / 6 / 4	9 / 9 / 4			
D												
E												
F												
G	1:1	1:2	1:4	1:8	1:16	1:32	1:64	1:128	1:256	1:512	1:1024	1:2048
H	1:1	1:2	1:4	1:8	1:16	1:32	1:64	1:128	1:256	1:512	1:1024	1:2048

*Note: All ug/ml concentrations subject to change.

*Key:

A-C/1-3	Capture antibody “low”, primary and secondary antibodies vary
A-C/4-6	Capture antibody “medium”, primary and secondary antibodies vary
A-C/7-9	Capture antibody “high”, primary and secondary antibodies vary
G	Monoclonal (Ab-1) as capture antibody, (C-20 as primary antibody) *Note: Does not produce great experimental results
H	Polyclonal (C-20) as capture antibody, (Ab-1 as primary antibody)
G & H	Dilution Ratios of Sample

*Additional Notes

Row G: Total amount of antibody needed = 1.2 ug Ab-1, 0.12 ug C-20, 0.0048 ug goat anti-rabbit HRP.

Row H: Total amount of antibody needed = 1.2 ug C-20, 0.06 ug Ab-1, 0.012 ug goat anti-rabbit HRP.